

Natural Quantum Monte Carlo Computation of Excited States

David Pfau^{1,2,*}, Simon Axelrod^{1,3,4}, Halvard Sutterud², Ingrid von Glehn¹, and James S. Spencer¹

¹*Google DeepMind, S2, 8 Handyside Street, London N1C 4DJ*

²*Department of Physics, Imperial College London, South Kensington Campus, London SW7 2AZ*

³*Department of Chemistry and Chemical Biology,
Harvard University, 12 Oxford St., Cambridge, MA 01238 and*

⁴*Department of Materials Science and Engineering,
Massachusetts Institute of Technology, 182 Memorial Dr., Cambridge, MA 01239*

(Dated: August 31, 2023)

We present a variational Monte Carlo algorithm for estimating the lowest excited states of a quantum system which is a natural generalization of the estimation of ground states. The method has no free parameters and requires no explicit orthogonalization of the different states, instead transforming the problem of finding excited states of a given system into that of finding the ground state of an expanded system. Expected values of arbitrary observables can be calculated, including off-diagonal expectations between different states such as the transition dipole moment. Although the method is entirely general, it works particularly well in conjunction with recent work on using neural networks as variational Ansätze for many-electron systems, and we show that by combining this method with the FermiNet and Psiformer Ansätze we can accurately recover vertical excitation energies and oscillator strengths on molecules as large as benzene. Beyond the examples on molecules presented here, we expect this technique will be of great interest for applications of variational quantum Monte Carlo to atomic, nuclear and condensed matter physics.

I. INTRODUCTION

The computation of excited states properties of quantum systems is a fundamental challenge in chemistry and many branches of physics. Understanding electronic excitations is critical for predicting photochemical phenomena such as fluorescence and conformational changes in the presence of light^{1,2}. In condensed matter physics, excitations determine the optical band gap of semiconductors, which is critical for predicting the behavior of solar cells, photosensors, LEDs and lasers³. Excited states are also relevant to understanding nuclear phenomena like metastable isomers and electron capture⁴. Ultimately, the dynamics of quantum systems when stimulated cannot be understood without taking excited states into account. Despite the importance of excited states for quantum phenomena, a full computational account of excited states remains challenging.

Quantum Monte Carlo (QMC) methods^{5,6} are an appealing class of algorithms for computing the behavior of quantum systems due to the favorable scaling with the number of particles, typically $\mathcal{O}(N^3) - \mathcal{O}(N^4)$, and wide applicability. Variational quantum Monte Carlo (VMC) in particular is quite conceptually simple, and consists of finding an explicit functional form for a wavefunction which minimizes a variational bound, but historically was not considered accurate enough on its own for many demanding applications. Recent work using neural networks as a wavefunction Ansatz has reinvigorated interest in VMC^{7,8}, and has demonstrated that VMC can be competitive with state-of-the-art methods for ground state calculations.

In this paper, we focus on computing excited states of quantum systems by VMC. When used to optimize ground states, there are only two variational principles

for QMC – energy minimization and variance minimization. Innovations in ground state VMC primarily focus on the choice of trial wavefunction^{9,10}, or optimization method used to achieve the variational bound^{11,12}, but the choice of objective to optimize is well-established. The same cannot be said for variational optimization of excited states.

Approaches for computing excited states by VMC can be broken down into several categories. Most methods are either *state-targeting*, in that they aim to find a single excited state, or *state-averaging*, in that they aim to find the lowest-lying exciting states by minimizing the total weighted energy of many states simultaneously. Among state-targeting methods, there are methods which target specific energy ranges^{13,14}, specific symmetries of the system¹⁵, or a specific ordering of the roots (i.e. the k -th lowest state)¹⁶. For state-averaging approaches, the different states must be kept orthogonal, which can be achieved by including a penalty term in the variational bound which pushes the states apart^{15,17,18}, or by explicitly constructing orthogonal Ansätze, sometimes repeatedly re-orthogonalizing during optimization^{19–22}.

All of these approaches have drawbacks and limitations. Targeting specific symmetries or energy ranges requires prior knowledge about the states of interest which may not be available, and state-targeting by variance minimization can lose track of the desired state²¹. Root-targeting methods are prone to root-flipping, whether they are used for QMC or other computational paradigms^{23,24}. Some methods require solving a generalized eigenvalue problem from stochastic estimates of the Hamiltonian and overlap matrices, which introduces biases into the gradients^{16,25}. Penalty methods often have problems with multiple Ansätze collapsing onto the same state, or have biased gradients¹⁸, and the

strength of the penalty term is a free parameter which must be chosen. Constructing orthogonal Ansätze is usually only possible when the Ansatz is a linear combination of basis set functions^{26,27}, which rules out many recently-developed Ansätze based on deep neural networks^{7,28–30}. Heuristics such as variance matching may be required to achieve good numerical results for all approaches. Despite almost four decades of work on QMC methods for excited states^{26,31}, no single variational principle has emerged which has no free parameters, has convergence guarantees when optimizing with noisy Monte Carlo estimates, and is applicable to all possible Ansätze and all excited states, regardless of symmetry.

Here we present a new variational principle for computing the lowest excited states of a quantum system by Monte Carlo which does not suffer from any of these limitations. Our method can be seen as a state-averaging approach with a particular choice of sampling distribution which does not require the states to be orthogonal. This choice of sampling distribution is equivalent to reformulating the problem of finding K excited states of an N particle system into the problem of finding the ground state of a K -fermion system where each fermion is equivalent to N particles in the original system. Instead of orthogonalizing the states, the local energy is promoted from a scalar to a matrix, which gives unbiased estimates of a matrix whose eigenvalues are the energies of orthogonal states. Because wavefunction optimization can be done by stochastic gradient descent from unbiased noisy estimates of the total energy, the procedure is guaranteed to converge to a local minimum of the total energy over states. Due to the many desirable mathematical properties which follow from the choice of sampling distribution, we refer to our proposed approach as *natural excited states* for VMC (NES-VMC).

II. METHOD

A. Variational Monte Carlo

First we briefly review ground-state VMC and establish some notation. We will stick to the notation of first quantization and consider a system of N particles with states $\mathbf{x} = \mathbf{x}_1, \dots, \mathbf{x}_N$, although everything we discuss could be applied to variational Ansätze represented in second quantization as well. We aim to find the lowest eigenfunction of a Hamiltonian operator \hat{H} . This can be done by reformulating the eigenfunction problem in variational form, as one of finding the minimum of the Rayleigh quotient:

$$\psi^* = \arg \min_{\psi} \frac{\langle \psi \hat{H} \psi \rangle}{\langle \psi^2 \rangle} \quad (1)$$

where the Ansatz ψ is not necessarily normalized. Computing this quotient involves taking high-dimensional in-

tegrals over all possible particle states \mathbf{x} , and can be approximated by Monte Carlo integration. Many choices of Monte Carlo sampling distribution $p(\mathbf{x})$ are possible, but if $p(\mathbf{x}) \propto \psi^2(\mathbf{x})$, then the Rayleigh quotient take a simple form that allows for unbiased empirical estimation of the energy and gradients of the energy:

$$\frac{\langle \psi \hat{H} \psi \rangle}{\langle \psi^2 \rangle} = \mathbb{E}_{\mathbf{x} \sim \psi^2} \left[\psi^{-1}(\mathbf{x}) \hat{H} \psi(\mathbf{x}) \right] \quad (2)$$

For this reason, ψ^2 is the natural choice of sampling distribution for ground state estimation. The scalar $E_L(\mathbf{x}) \triangleq \psi^{-1}(\mathbf{x}) \hat{H} \psi(\mathbf{x})$ that appears inside the expectation is the *local energy*, and at any eigenfunction of \hat{H} it will be constant if \hat{H} is a local operator.

B. Natural Excited States

Going from ground states to excited states, we aim to find the lowest K eigenfunctions of \hat{H} . We refer to a single set of N particle states as a *particle set*, and denote different particle sets with an upper index, so that \mathbf{x}^i denotes a set of N particles $\mathbf{x}_1^i, \dots, \mathbf{x}_N^i$. For the remainder of the article, we will use \mathbf{x} to denote the complete state of all particle sets $\mathbf{x}^1, \dots, \mathbf{x}^K$. Let ψ_i denote a (possibly unnormalized) N -particle wavefunction, then we are trying to find wavefunctions ψ_1, \dots, ψ_K which approximate the lowest excited states. Let $\Psi(\mathbf{x}) \in \mathbb{R}^{K \times K}$ denote the matrix combining all electron sets with all wavefunctions:

$$\Psi(\mathbf{x}) \triangleq \begin{pmatrix} \psi_1(\mathbf{x}^1) & \dots & \psi_K(\mathbf{x}^1) \\ \vdots & & \vdots \\ \psi_1(\mathbf{x}^K) & \dots & \psi_K(\mathbf{x}^K) \end{pmatrix} \quad (3)$$

The determinant of this matrix $\Psi(\mathbf{x}) = \det(\Psi(\mathbf{x}))$ can be thought of as an unnormalized Slater determinant, except that instead of single-particle orbitals, it is made up of N -particle wavefunctions. We call $\Psi(\mathbf{x}) = \det(\Psi(\mathbf{x}))$ the *total Ansatz*, while the individual ψ_i are the *single-state Ansätze*.

Rather than optimizing the single-state Ansätze in order from lowest to highest energy, we will only optimize the total Ansatz to minimize the total energy of all states. This is conceptually quite similar to state-averaging approaches in VMC, except that we will not explicitly enforce the orthogonality of the different single-state Ansätze. Note that taking any linear combination of single-state Ansätze $\psi'_i = \sum_j a_{ij} \psi_j$ only changes the total Ansatz by a constant factor. Also note that if two single-state Ansätze are the same, the total Ansatz becomes zero. Thus, by representing the total Ansatz as a determinant of single-state Ansätze, we can prevent the collapse of different Ansätze onto the same state, without requiring them to be orthogonal.

For an arbitrary operator \hat{O} that acts on N -particle wavefunctions, let $\hat{O}\Psi(\mathbf{x})$ denote the matrix of all values

of this operator applied to all single-state Ansätze and particle sets:

$$\hat{\mathcal{O}}\Psi(\mathbf{x}) \triangleq \begin{pmatrix} \hat{\mathcal{O}}\psi_1(\mathbf{x}^1) & \dots & \hat{\mathcal{O}}\psi_K(\mathbf{x}^1) \\ \vdots & & \vdots \\ \hat{\mathcal{O}}\psi_1(\mathbf{x}^K) & \dots & \hat{\mathcal{O}}\psi_K(\mathbf{x}^K) \end{pmatrix} \quad (4)$$

Let \mathbf{S} and $\hat{\mathcal{O}}$ denote the overlap matrix between states and the matrix of expectations of states for the operator $\hat{\mathcal{O}}$:

$$\mathbf{S} \triangleq \begin{pmatrix} \langle \psi_1^2 \rangle & \dots & \langle \psi_1 \psi_K \rangle \\ \vdots & & \vdots \\ \langle \psi_K \psi_1 \rangle & \dots & \langle \psi_K^2 \rangle \end{pmatrix} \quad (5)$$

$$\hat{\mathcal{O}} \triangleq \begin{pmatrix} \langle \psi_1 \hat{\mathcal{O}} \psi_1 \rangle & \dots & \langle \psi_1 \hat{\mathcal{O}} \psi_K \rangle \\ \vdots & & \vdots \\ \langle \psi_K \hat{\mathcal{O}} \psi_1 \rangle & \dots & \langle \psi_K \hat{\mathcal{O}} \psi_K \rangle \end{pmatrix} \quad (6)$$

If \hat{H} is the Hamiltonian for the system under consideration, then we can define an expanded Hamiltonian that acts on the total Ansatz Ψ as $\hat{\mathcal{H}} = \hat{H}_1 \oplus \dots \oplus \hat{H}_K$, where \hat{H}_i is the Hamiltonian that acts only on particle set i . The ground state energy of $\hat{\mathcal{H}}$ is the sum of the lowest K energies of \hat{H} , and the ground state wavefunction Ψ^* is a determinant of the K lowest states $\psi_1^*, \dots, \psi_K^*$ of \hat{H} . This can be seen by writing out the Rayleigh quotient for the total Ansatz and expanded Hamiltonian:

$$\begin{aligned} \frac{\langle \Psi \hat{\mathcal{H}} \Psi \rangle}{\langle \Psi^2 \rangle} &= \frac{\langle \Psi \hat{\mathcal{H}} \Psi \rangle}{\det(\mathbf{S})} = \frac{\sum_i \langle \Psi \hat{H}_i \Psi \rangle}{\det(\mathbf{S})} \\ &= \frac{\sum_i \det \begin{pmatrix} \langle \psi_1^2 \rangle & \dots & \langle \psi_1 \hat{H}_i \psi_i \rangle & \dots & \langle \psi_1 \psi_K \rangle \\ \vdots & & \vdots & & \vdots \\ \langle \psi_K \psi_1 \rangle & \dots & \langle \psi_K \hat{H}_i \psi_i \rangle & \dots & \langle \psi_K^2 \rangle \end{pmatrix}}{\det(\mathbf{S})} \end{aligned} \quad (7)$$

The terms in the numerator are rank-one updates to the denominator, and using the matrix determinant lemma, Eq. 7 can be rewritten as

$$\frac{\langle \Psi \hat{\mathcal{H}} \Psi \rangle}{\langle \Psi^2 \rangle} = \text{Tr} \left[\mathbf{S}^{-1} \hat{\mathbf{H}} \right] \quad (8)$$

The minimum of the expression in Eq. 8 is a set of functions $\psi_1^*, \dots, \psi_K^*$ that span the bottom K eigenfunctions of \hat{H} . However, note that we have no way to know from this expression alone how to decompose the total energy into individual energies.

To minimize the objective function in Eq. 7, we can do conventional energy minimization for VMC. The Rayleigh quotient can be rewritten as an expectation of the local (total) energy:

$$\mathbb{E}_{\mathbf{x} \sim \Psi^2} \left[\Psi^{-1}(\mathbf{x}) \hat{\mathcal{H}} \Psi(\mathbf{x}) \right] = \text{Tr} \left[\mathbb{E}_{\mathbf{x} \sim \Psi^2} \left[\Psi^{-1}(\mathbf{x}) \hat{\mathbf{H}} \Psi(\mathbf{x}) \right] \right] \quad (9)$$

where in the last expression we have again used the matrix determinant lemma to rewrite the objective in terms of the single-state Ansätze, as well as the linearity of the trace to move it outside the expectation. A more thorough derivation is given in Sec. A. Here we generate samples of K electron sets simultaneously (or equivalently, NK particles) by sampling from a density proportional to Ψ^2 . Unbiased gradients of this objective function can be computed as in standard VMC and plugged into any number of gradient-based optimization algorithms.

This is clearly a direct generalization of the VMC objective in Eq. 2. In the same way that ψ^2 is the natural choice of sampling distribution for ground state VMC, we believe that Ψ^2 is the natural choice of sampling distribution for state-averaged excited-state VMC. We define the *local energy matrix* to be the term inside the expectation in Eq. 9:

$$\mathbf{E}_L(\mathbf{x}) \triangleq \Psi^{-1}(\mathbf{x}) \hat{\mathbf{H}} \Psi(\mathbf{x}) \quad (10)$$

When $K = 1$ this reduces to the scalar local energy in Eq. 2. The benefits of this choice of sampling distribution go beyond the simple functional form of $\mathbf{E}_L(\mathbf{x})$, and we will see that this matrix in fact contains all the information needed to compute the full spectrum of energies.

Note that the expression in Eq. 9 looks quite similar to Eq. 8. Not only are the traces of $\mathbf{S}^{-1} \hat{\mathbf{H}}$ and $\mathbb{E}_{\Psi^2}[\mathbf{E}_L(\mathbf{x})]$ equal, but in fact the two matrices are identical. This can be seen by following the same derivation as in Eqs. 7-9, but rather than with the operator $\hat{\mathcal{H}}$, with an operator \hat{H}_{ij} such that $\hat{H}_{ij} \psi_k(\mathbf{x}^i) = \hat{H} \psi_k(\mathbf{x}^j)$ and is the identity for all other \mathbf{x}^i . Plugging in this operator to the Rayleigh quotient, one can show that it gives row i and column j in $\mathbf{S}^{-1} \hat{\mathbf{H}}$, while plugging it into the Monte Carlo form of the objective gives row i and column j of $\mathbb{E}_{\Psi^2}[\mathbf{E}_L(\mathbf{x})]$

While we only need to use the diagonal of the matrix $\mathbb{E}_{\Psi^2}[\mathbf{E}_L(\mathbf{x})]$ for optimization, the full matrix has precisely the information which we need to separate the different excited states in proper order. When we plug in the exact eigenfunctions $\psi_1^*, \dots, \psi_K^*$, we find that $\Psi^{*-1} \hat{\mathbf{H}} \Psi^* = \Psi^{*-1} \Psi^* \mathbf{\Lambda} = \mathbf{\Lambda}$, where $\mathbf{\Lambda}$ is the diagonal matrix of energies, and even if the single-state Ansätze are linear combinations of eigenfunctions $\psi_i = \sum_j a_{ij} \psi_j^*$, then $\Psi^{*-1} \hat{\mathbf{H}} \Psi^* = \mathbf{A}^{-1} \mathbf{\Lambda} \mathbf{A}$. This suggests that, if we are in the vicinity of the true ground state of the total Ansatz, then by accumulating and then diagonalizing the matrix $\mathbb{E}_{\Psi^2}[\mathbf{E}_L(\mathbf{x})] = \mathbf{U} \mathbf{\Lambda} \mathbf{U}^{-1}$, we can recover the individual energies of the states in order, rather than simply the total energy. Note that in general $\mathbf{U} = \mathbf{A}^{-1} \mathbf{\Sigma}$ where $\mathbf{\Sigma} = \begin{pmatrix} \sigma_1 & & \\ & \ddots & \\ & & \sigma_K \end{pmatrix}$ is an arbitrary diagonal matrix which is not identifiable.

Not only is diagonalizing $\mathbb{E}_{\Psi^2}[\mathbf{E}_L(\mathbf{x})]$ sufficient to recover the energies – it also provides us with the necessary change of basis to evaluate other observables \hat{O} , even off-diagonal observables $\langle \psi_i \hat{O} \psi_j \rangle$ between states. This can be seen due to the identity $\mathbb{E}_{\Psi^2}[\Psi^{-1} \hat{O} \Psi] = \mathbf{S}^{-1} \hat{O}$, and for single-state Ansätze which are a linear combination of eigenfunctions, $\mathbf{S}^{-1} \hat{O} = \mathbf{A}^{-1} \hat{O}^* \mathbf{A}$. So if we accumulate and diagonalize $\mathbb{E}_{\Psi^2}[\mathbf{E}_L(\mathbf{x})]$ and use the resulting eigenvectors to compute $\mathbf{U}^{-1} \mathbb{E}_{\Psi^2}[\Psi^{-1} \hat{O} \Psi] \mathbf{U}$, then in the vicinity of the true ground state of the total Ansatz the result will be approximately $\Sigma^{-1} \hat{O}^* \Sigma$. Along the diagonal, this gives exactly the expectations $\langle \psi_i^* \hat{O} \psi_i \rangle$. Off the diagonal, this yields $\frac{\sigma_i}{\sigma_j} \langle \psi_i^* \hat{O} \psi_j \rangle$. If we multiply the matrix elementwise by its transpose, the σ_i terms cancel out, and we recover $\langle \psi_i^* \hat{O} \psi_j \rangle^2$, which gives the expectation up to a sign factor. This sign factor is not physically observable however, and in practice for computing quantities like the oscillator strength, only the expectation squared is needed.

C. Neural Network Ansätze

The use of variational Monte Carlo for ground state calculations was typically used to find a trial wavefunction for more accurate projector QMC methods like diffusion Monte Carlo⁵ or auxiliary field Monte Carlo³³. However, in recent years, advances in deep neural networks have led to their use as accurate Ansätze for studying spin systems⁷, electronic structure⁸ and nuclear systems³⁴, often reaching levels of accuracy rivaling projector QMC methods. This has led to a renewed interest in VMC as a standalone method. While a variety of different neural network architectures can be used depending on the problem, such as restricted Boltzmann machines⁷, convolutional neural networks³⁵, and autoregressive models³⁶, a number of custom architectures have been developed specifically for many-body electronic structure problems in first quantization^{28–30,37–41}. Most of these Ansätze start from a linear combination of Slater determinants:

$$\psi(\mathbf{x}) = \sum_k \omega_k \det \begin{pmatrix} \phi_1^k(\mathbf{x}_1) & \dots & \phi_N^k(\mathbf{x}_1) \\ \vdots & & \vdots \\ \phi_1^k(\mathbf{x}_N) & \dots & \phi_N^k(\mathbf{x}_N) \end{pmatrix} \quad (11)$$

It has long been recognized⁴² that the single-particle orbitals in a Slater determinant can be generalized to depend on *all* particles, so long as they depend on all but one in a permutation-independent manner:

$$\psi(\mathbf{x}) = \sum_k \omega_k \det \begin{pmatrix} \phi_1^k(\mathbf{x}_1; \{\mathbf{x}_{/1}\}) & \dots & \phi_N^k(\mathbf{x}_1; \{\mathbf{x}_{/1}\}) \\ \vdots & & \vdots \\ \phi_1^k(\mathbf{x}_N; \{\mathbf{x}_{/N}\}) & \dots & \phi_N^k(\mathbf{x}_N; \{\mathbf{x}_{/N}\}) \end{pmatrix} \quad (12)$$

where $\{\mathbf{x}_{/i}\}$ denotes the set of all particles *except* \mathbf{x}_i . In the event that the particles are spin-assigned, the orbitals can also be expressed as $\phi_i^k(\mathbf{x}_j^\uparrow; \{\mathbf{x}_{/j}^\uparrow, \{\mathbf{x}^\downarrow\})$ where

the function is only invariant to changing the order of particles of the same spin. Most neural network Ansätze for electrons in real space implement this idea by using permutation-equivariant deep neural networks to represent the orbitals, sometimes with a multiplicative Jastrow factor to account for pairwise interactions^{29,30,38}.

Extending these Ansätze to represent multiple states is quite straightforward. Each state is still expressed as a sum of determinants of generalized neural network orbitals, there are simply more orbitals:

$$\psi_i(\mathbf{x}) = \sum_{ik} \omega_{ik} \det \begin{pmatrix} \phi_1^{ik}(\mathbf{x}_1; \{\mathbf{x}_{/1}\}) & \dots & \phi_N^{ik}(\mathbf{x}_1; \{\mathbf{x}_{/1}\}) \\ \vdots & & \vdots \\ \phi_1^{ik}(\mathbf{x}_N; \{\mathbf{x}_{/N}\}) & \dots & \phi_N^{ik}(\mathbf{x}_N; \{\mathbf{x}_{/N}\}) \end{pmatrix} \quad (13)$$

Nothing is changed about the neural network architecture itself, just the number of orbitals is increased proportionally to the number of states.

Neural network Ansätze differ from classic Ansätze like the Slater-Jastrow-backflow Ansatz⁹ in important ways which make it difficult to apply existing excited state methods. Many methods assume that the Ansatz is a linear combination of orthogonal basis functions like Slater determinants, a necessary assumption for maintaining the orthogonality of states, either through explicit construction or a diagonalization step¹⁹. Classic Ansätze are usually optimized through a small number of gradient steps, where each gradient step is accumulated over a large number of MCMC steps, so that the gradients are nearly deterministic. Most modern deep neural networks, by contrast, are optimized by stochastic gradient descent using a large number of small, noisy steps⁴³. This means bias in the gradients becomes a more significant concern.

Existing work on excited state calculations with neural networks has focused on penalty methods^{15,18}, but these still require choosing a free parameter trading off total energy and penalty strength, and may not exactly satisfy orthogonality in the states. Some of these methods also have biased gradients in the penalty term¹⁸ due to nonlinearities meant to push states apart more strongly. By contrast, the NES-VMC method has no free parameters to tune, can be optimized by unbiased gradients that have the same form as for ground state calculations, does not require the states to be orthogonal, and makes no assumption on the functional form of the Ansatz. Thus, while NES-VMC is generally applicable to *all* excited state VMC calculations, it is particularly well-tailored for use with recently developed neural network Ansätze.

III. RESULTS

While the natural excited states method is fully general and can be applied to any quantum Hamiltonian, our experimental validation is focused on electronic structure in atoms and molecules, due to the abundant experimental and computational literature to compare against. For

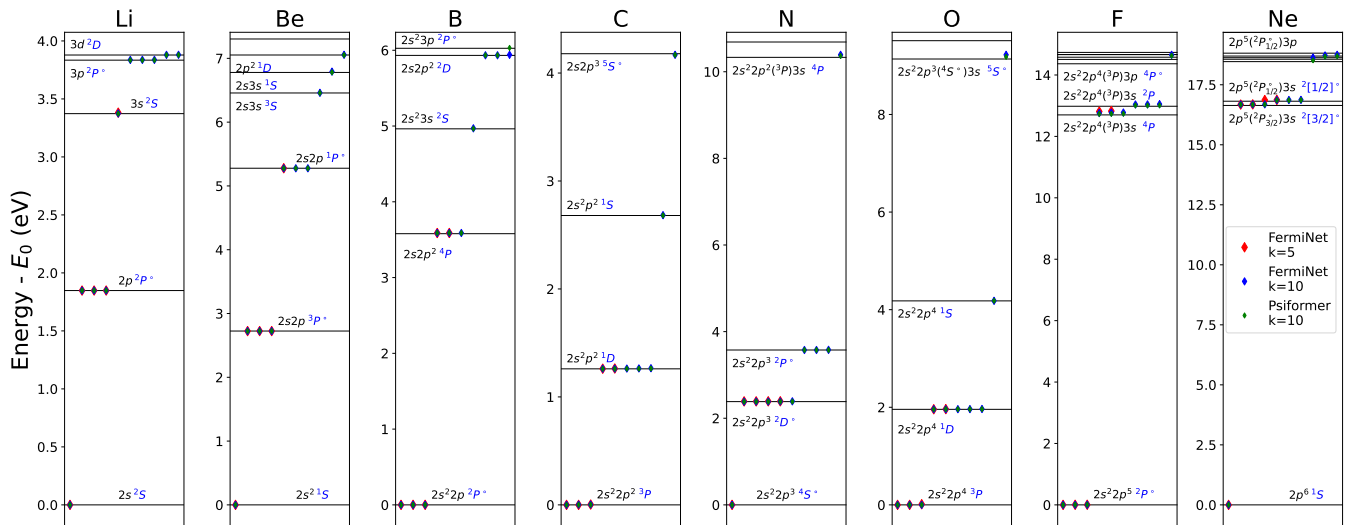


FIG. 1: Excited state energies for first row atoms from lithium to neon. Results from natural excited state VMC applied to the FermiNet (10 states, blue, 5 states, red) are shown on top of experimental results³². Spectral lines which match computed states are labeled with electron configurations and atomic term symbols (except for the highest levels of F and Ne, where term symbols are omitted for clarity). For all but the largest systems and highest excited states, there is excellent agreement with experiment. The discrepancy between 5 and 10 excited states is minimal except for the highest excited states of F and Ne, where computing more states increases the accuracy of a given state. Complete numerical results are given in Table II.

all experiments, we are solving the Schrödinger equation in the Born-Oppenheimer approximation⁴⁴:

$$\hat{H} = -\frac{1}{2} \sum_i \nabla_i^2 + \sum_{i>j} \frac{1}{|\mathbf{r}_i - \mathbf{r}_j|} - \sum_{iI} \frac{Z_I}{|\mathbf{r}_i - \mathbf{R}_I|} + \sum_{I>J} \frac{Z_I Z_J}{|\mathbf{R}_I - \mathbf{R}_J|} \quad (14)$$

where the indices i and j are over electrons and I and J are over atomic nuclei with fixed locations.

To try to disentangle the effect that the choice of Ansatz has on performance, we investigated two different neural network architectures: the Fermionic Neural Network (FermiNet)²⁹ and the Wavefunction Transformer (Psiformer)³⁸. While the Psiformer has generally been found to be more accurate on large systems, it is also slower, and for ground state calculations up to approximately 15 electrons, no appreciable difference in accuracy between the two has been found.

A. Atomic Spectra

As an initial check of the correctness of our method, we investigate the excited states of first-row atoms, from lithium to neon. Atomic spectral lines have been the subject of some of the highest-precision measurements in all of science, and while we do not aim to reach spectroscopic accuracy, we can have high confidence in accuracy

of the measurements, and do not need to worry about effects such as adiabatic relaxation and zero-point vibrational energy which affect molecular measurements. All experimental data was taken from the energy level tables in the NIST Handbook of Basic Atomic Spectroscopic Data³². Because we are working with the nonrelativistic Schrödinger equation without spin-orbit corrections, we are not able to compute fine or hyperfine structure. To remove the fine structure, experimental energy levels with different total angular momenta are averaged together weighted by the degeneracy $m_J = 2J + 1$ and treated as a single level. The hyperfine structure is too small to be of concern here. To investigate the effect of the choice of Ansatz as well as the choice of number of states k to compute, we ran calculations with the FermiNet with both 5 and 10 states, as well as the Psiformer with 10 states. Results are given in Fig. 1, with numerical results (including error bars) in the Appendix in Table II.

For all atoms, NES-VMC gives results closely matching experiment. From lithium up to oxygen, the error relative to experiment is far less than 1 mHa (27.2 meV) for all but the highest excited state, and is often less than 0.1 mHa, an exceedingly high level of accuracy for a deep neural network Ansatz. On lithium, all Ansätze correctly converge to the 2S and $^2P^\circ$ states, which are missed by the PauliNet penalty method¹⁸. The method struggles in some cases to get the highest energy state correct, but this seems to be improved by simply computing more states – for instance, the error in the 4P states of fluorine is cut in half by increasing the number of states from 5 to 10. In rare cases, the highest state

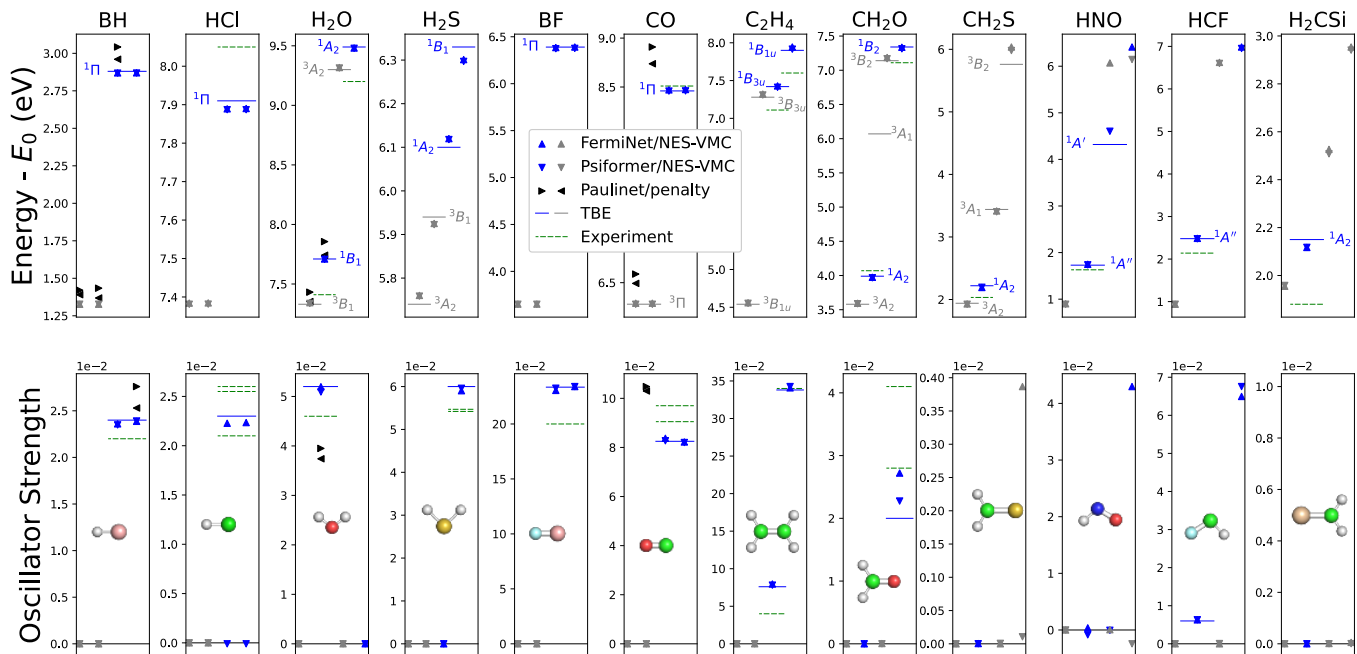


FIG. 2: Vertical excitation energies and oscillator strengths for small molecules from Chrayteh *et al.*⁴⁵. Singlet states are in blue and triplet states are in gray. NES-VMC results are indicated by markers while theoretical best estimates from Chrayteh *et al.*⁴⁵ or directly from QUEST⁴⁶ are given by the lines. When no data from QUEST is available, no TBE is given. Experimental results from Chrayteh *et al.*⁴⁵ and references therein are given by the dashed lines in green. Where available, energies and oscillator strengths from Entwistle *et al.*¹⁸ are provided by the black triangles for comparison, with (pointing left) and without (pointing right) variance matching. In most cases, our results on both energies and oscillator strengths agree closely with theoretical best estimates. Complete numerical results are given in Table III.

seems to converge to the incorrect state, such as boron with the Psiformer, which seems to converge to the $^2P^o$ state rather than the last 2D state. Fluorine and neon both have relatively large errors on the order of 1-2 mHa for low-lying states, but going from the FermiNet to the more accurate Psiformer Ansatz seems to reduce this error in all cases. The largest errors are in the highest states of fluorine and neon, where the error is significant. In this case we suspect the difficulty is due to the large number of different states with similar electron configurations and energies, and hope that by computing even more states or by using even more expressive Ansätze, the effects of individual states can be disentangled. The excellent performance on low-lying states gives us confidence that NES-VMC is mathematically sound.

B. Oscillator Strengths

Going beyond results on single atoms and vertical excitation energies, we are interested in the performance of NES-VMC on more complicated molecular systems, as well as observable quantities other than the energy. The QUEST database^{45,46,48-54} is an excellent source of well-controlled benchmark vertical excited states calculations using coupled cluster methods on molecules

of various sizes, with consistent geometries and basis set extrapolations. Of particular interest is the subset of QUEST for which oscillator strengths have been computed⁴⁵, as oscillator strengths provide a strong test of how well an excited state method can perform on experimentally-observable quantities, and especially as oscillator strength and transition probability calculations are known to be highly sensitive to choices of basis set⁵⁵.

Oscillator strengths are a measure of the probability of transition between different states occurring as a result of photon emission or absorption. Under the assumption that the wavelength of the photon is much longer than the system under consideration, so the interaction can be approximated by a constant electric field, the transition dipole moment between two states gives a measure of how that transition will interact with light:

$$\mathbf{d}_{ij} = \left\langle \psi_i^\dagger \sum_k q_k \mathbf{r}_k \psi_j \right\rangle \quad (15)$$

where the sum over k is taken over all particles in the system with charge q_k and position \mathbf{r}_k . For electrons, $q_k = -e$. The transition dipole moments are vector-valued quantities which include a complex phase factor, and are not directly observable. The oscillator strength

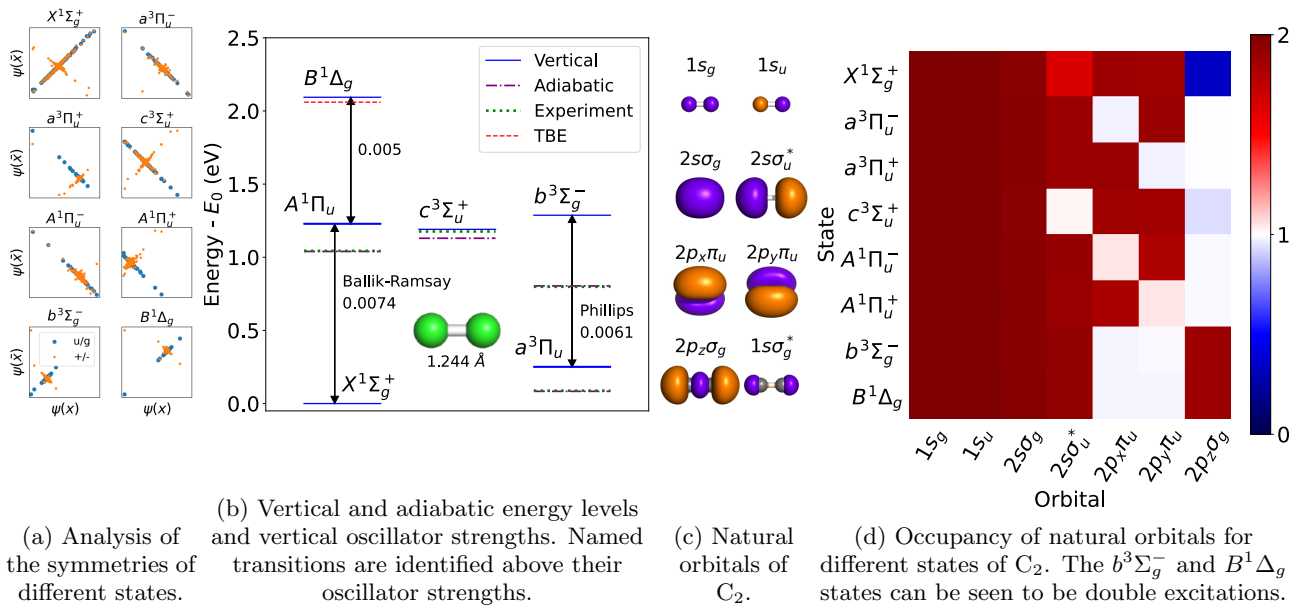


FIG. 3: Excited states of the carbon dimer (C_2). (a) The symmetries of the different states can be identified by evaluating each single state Ansatz at location \mathbf{r} and $-\mathbf{r}$ for parity symmetry (u/g, blue) or by flipping \mathbf{r} across the x -axis for reflection symmetry (+/-, orange). (b) The vertical and adiabatic energies of excited states of C_2 . The green line indicates experimental energies⁴⁷ and the red line indicates the energy of the $B^1\Delta_g$ state from QUEST⁴⁸. Bright transitions are labelled with their oscillator strength and, when available, their names. (c) Visualization of the 8 lowest natural orbitals of C_2 . (d) The occupancy of the different natural orbitals for the different excited states of C_2 , identified from the density matrix of each state. The $a^3\Pi_u$ through $A^1\Pi_u$ states are single excitations while the last two states are double excitations. Complete numerical results are given in Table IV.

of a particular transition can be computed from the transition dipole moment:

$$f_{ij} = \frac{2}{3} \frac{m}{\hbar^2} (E_i - E_j) |\mathbf{d}_{ij}|^2 \quad (16)$$

which reduces the transition dipole moment to a dimensionless positive scalar. In natural excited states, we can compute expectations of operators between different states up to an arbitrary sign factor, and that sign factor goes away in the oscillator strength. Computational details are discussed in more detail in Sec. C 3.

We applied NES-VMC to all of the small molecules investigated in Chrayteh *et al.*⁴⁵, computing the 5 lowest energy states with both the FermiNet and Psiformer. Results are presented in Fig. 2 and Table III. Wherever possible, we take results from QUEST^{45,46} to be theoretical best estimates (TBEs) for comparison, though for many of the states we converged to, especially triplets, no results exist in QUEST. For molecules with heavier atoms (HCl, H_2S , H_2CSi), we found that using pseudopotentials for the heaviest atoms significantly improved the accuracy of the results, likely because the total energy scale was reduced by ignoring core electrons. Where applicable, we also include a comparison against the VMC penalty method of Entwistle *et al.*¹⁸. We omit N_2 because the lowest-lying excited states are all triplets. For all diatomic systems, the $^1\Pi$ state is doubly-degenerate,

and so the baseline oscillator strengths are divided by two to match the computed results.

In almost all cases, both the vertical excitation energies and the oscillator strengths are in excellent agreement with the TBE. The vertical excitation energies are almost all within chemical accuracy (1.6 mHa or 0.04 eV) of the TBE while the oscillators strengths usually diverge from the TBE by at most an amount on the order of 0.001, comparable to the uncertainty in the calculations. The results of Entwistle *et al.*, in contrast, often differ noticeably from other theoretical results, even when correction using variance matching are applied. This is particularly noticeable for the oscillator strengths. We note that we do not use variance matching for any of the NES-VMC calculations.

There are a few cases where NES-VMC behaves oddly. While the FermiNet and Psiformer find nearly identical vertical excitation energies for the $^1\Pi$ state of HCl, and the FermiNet accurately predicts the oscillator strength, the Psiformer mistakenly finds this to be a dark state. On formaldehyde (CH_2O), both the FermiNet and Psiformer fail to find the 3A_1 state at all, and the oscillator strength for the 1B_2 state diverges from the TBE by a significant margin, although the Psiformer halves that margin relative to the FermiNet. Vertical excitation energies for systems with heavier atoms, such as H_2S , and the highest state of thioformaldehyde (CH_2S), are not quite

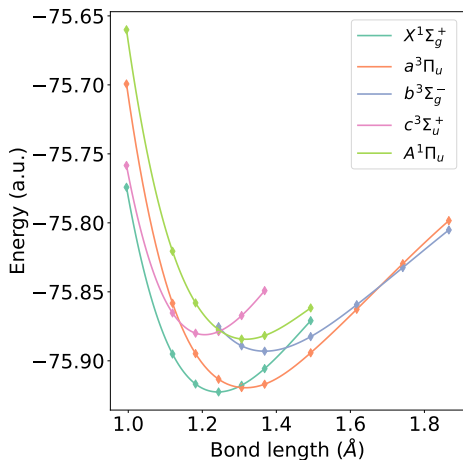


FIG. 4: Potential energy curves of the low-lying excited states of C_2 which can be uniquely identified from their symmetries. Complete numerical results are given in Table V.

as accurate as other results, though in the case of thioformaldehyde we are hopeful that, consistent with the atomic results in the previous section, computing more states will reduce the error in the 3B_2 state. For nitroxyl (HNO), the FermiNet fails to converge to the $^1A'$ state, but the Psiformer finds it correctly, albeit with a relatively large error in the vertical excitation energy. This suggests that there are occasional difficulties in getting NES-VMC to converge to all low-lying states, but we are hopeful that improvements in optimization methods can improve this in the future. What is clear is that NES-VMC works well in the large majority of cases, and is far more accurate than alternative methods which have been proposed for neural network Ansätze.

Other QMC methods have also been applied to some of these systems. In particular, the QMC-CIPSI method has been successfully applied to computing the vertical excitation energies of the 1A_2 state in formaldehyde and thioformaldehyde to within chemical accuracy, using a conventional Slater-Jastrow Ansatz⁵⁶. While the QMC-CIPSI method cannot be applied to neural network Ansätze, this suggests that good results can still be achieved with VMC with a simple Ansatz, and that the benefit of using NES-VMC relative to the penalty method in Entwistle *et al.* is due to the method rather than the choice of Ansatz.

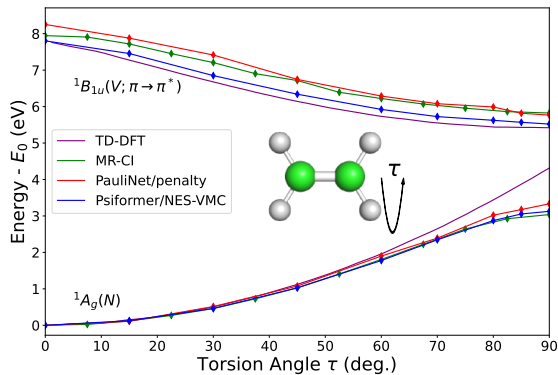
C. Carbon Dimer

In addition to computing observable quantities, it is also desirable to be able to say something about the *nature* of different excited states – whether a state is a valence or Rydberg or charge transfer excitation, what its symmetries are, whether it is a single or double excitation, etc. As a benchmark system for demonstrating the

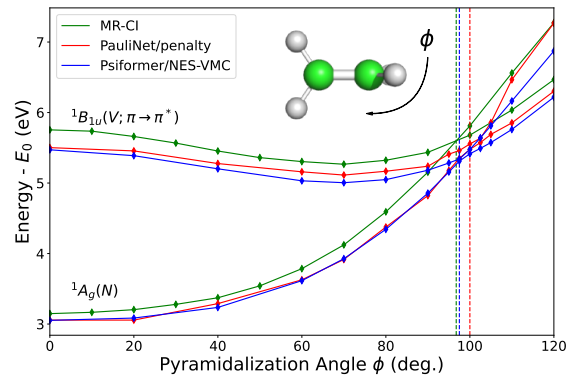
ability of NES-VMC to characterize different states, we study the carbon dimer (C_2). Despite its small size, the carbon dimer has a complicated electronic structure with a large number of low-lying excited states^{47,59,60}. Due to the existence of very strong bands in the visible spectrum, the carbon dimer is frequently detected in astrophysical measurements, and can be observed in comets rich in organic materials⁶¹. The exact bond order of C_2 is still a subject of some controversy – while molecular orbital theory would classify it as a double bond, valence bond calculations suggest it may be better described as a quadruple bond⁶². And the carbon dimer is one of the smallest molecules to have low-lying double excitations, a class of excited state which other methods often struggle with⁴⁸. Correctly reconstructing the potential energy curves for different low-lying states requires correctly disentangling and characterizing these different states at different geometries.

We compute the 8 lowest-lying states of the carbon dimer at several different bond lengths using NES-VMC and the Psiformer Ansatz, and present the results in Figs. 3 and 4. At equilibrium (1.244 Å), we classify the different states by computing their spin magnitude and their symmetries – both parity symmetry (u/g) where the electron positions \mathbf{r} are replaced by $-\mathbf{r}$ and reflection symmetry (+/-) where the positions are flipped on the x-axis. We do not compute the orbital angular momentum operator, but confirm that we see the expected degeneracy, for instance Π states are doubly degenerate (one of each reflection symmetry). The oscillator strengths show several bright transitions, which we show in Fig. 3b. Due to the degeneracy of the Π states, we add the oscillator strengths together to give the total strength. We correctly identify the Phillips and Ballik-Ramsay systems^{63,64}, as well as the unnamed $B^1\Delta_g \rightarrow A^1\Pi_u$ transition. We also find that the energy of the $B^1\Delta_g$ energy closely matches the TBE in QUEST⁴⁸. The $A^1\Pi_u$, $c^3\Sigma_u^+$ and $b^3\Sigma_g^-$ states all have nearly the same energy, so correctly identifying the oscillator strengths for these transitions is very challenging.

To better understand the nature of each excited state, we compute the occupancy of the different natural orbitals. We first compute the one-electron reduced density matrix (1-RDM) for each single-state Ansatz in a large basis set and then diagonalize these matrices to find the natural orbitals, as described in more detail in Sec. C 2. In this case, using the Hartree-Fock orbitals as the basis set, we find that all 1-RDMs are nearly diagonal, that is the natural orbitals closely match the Hartree-Fock molecular orbitals. We see in Fig. 3d that all states above the ground state involve excitation of electrons into the $2p_z\sigma_g$ orbital. The Π states are well-described by single excitations from one of the $2p\pi_u$ orbitals while the $c^3\Sigma_u^+$ state promotes an electron from the $2s\sigma_u^*$ orbital. Finally, both the $b^3\Sigma_g^-$ and $B^1\Delta_g$ states are double excitations of the $2p\pi_u$ electrons into the $2s\sigma_u^*$ orbital, as expected. Not only is NES-VMC able to predict double excitation energies correctly, but by having an explicit functional form



(a) Potential energy curve of the first two singlet states of ethylene under torsion around the C-C bond.



(b) Potential energy curve of the first two singlet states of ethylene under pyramidalization of the C-H bonds.

FIG. 5: Excited states and conical intersection of ethylene (C_2H_4). Our results (blue) are compared against TD-DFT⁵⁷ (purple), MR-CI⁵⁸ (green) and a penalty method used with the PauliNet¹⁸ (red). The best estimate of the location of the conical intersection of the V and N states for each method is given by the vertical line in Fig. 5b. Our method is in close agreement with MR-CI up to a constant shift, and agrees with the location of the conical intersection better than the PauliNet penalty method. Note that the $\phi = 0$ geometry in Fig. 5b differs slightly from the $\tau = 90$ geometry in Fig. 5a, as in Barbatti *et al.*⁵⁸. Complete numerical results are given in Table VI.

for the wavefunction Ansatz, we can compute quantities such as the reduced density matrices which allow us to derive insight about the nature of electronic excitations.

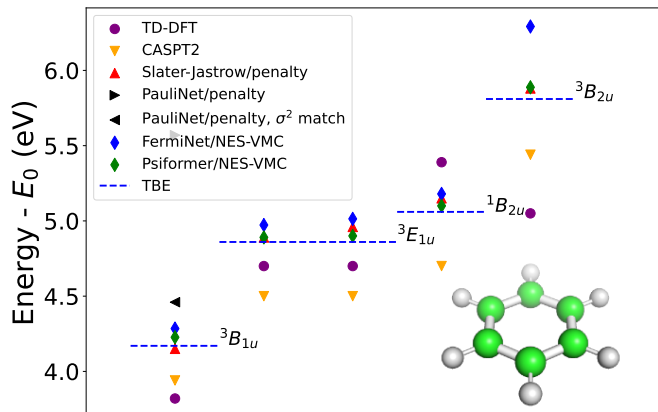
Predicting experimental excitation energies requires computing the energy difference between different states in their respective lowest energy configurations, the so-called *adiabatic* excitation energy. To compute this for C_2 , we repeated the equilibrium calculations at a number of different bond lengths. Wherever possible, we matched the energy levels at different geometries to the appropriate states based on the same symmetries as in Fig 3a, and for five states we were able to reconstruct enough of the potential energy curve to identify the minimum energy for each. The results are shown in Fig. 4, smoothed by cubic interpolation. Taking the difference between the minimum energies of each state gives an estimate of the adiabatic excitation energy, which we show in purple in Fig. 3b, and in 3 out of 4 cases we matched the experimental energy⁴⁷ to within roughly 0.01 eV. We did not estimate the zero-point vibrational energies, but believe this may explain the discrepancy in the $c^3\Sigma_u^+$ state. This shows that not only can NES-VMC match other theoretical calculations of vertical excitation energies, but can predict experimental results to high accuracy.

D. Twisted Ethylene

The excited states of ethylene (C_2H_4) across its potential energy surface present a challenging benchmark problem for many methods. As the torsion of the carbon double bond is increased, an avoided crossing occurs when the torsion angle is 90° . Even for ground state cal-

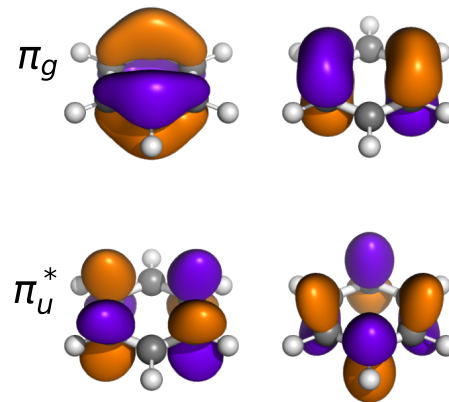
culations, DFT and single-reference coupled cluster calculations predict an unphysical cusp at this location⁶⁷. Starting from the 90° torsion and bending the hydrogen atoms on one side inward (so-called “pyramidalization”), ethylene undergoes a conical intersection where the ground state transitions from a π to π^* highest occupied orbital (the N and V states, with term symbols 1A_g and $^1B_{1u}$). Modeling this conical intersection requires fundamentally multireference methods, and while time-dependent density functional theory (TD-DFT) struggles with this system⁶⁸, multireference configuration interaction (MR-CI) methods describe it well⁵⁸.

We compute the excited states of ethylene as the torsion angle is varied from 0° to 90° , followed by variation of the pyramidalization angle from 0° to 120° , enough to include the conical intersection of the N and V states. We try to match the geometry from previous MR-CI studies⁵⁸ as closely as possible. Results are shown in Fig. 5. There are also several low-lying triplet states of ethene, the $^3B_{1u}$ and $^3B_{3u}$ states, and so we calculated $K = 3$ excited states for all geometries, which we found was enough to find two singlet states for all geometries except at equilibrium, where we used $K = 5$ and took the highest state, as the $^1B_{3u}$ state has lower energy exclusively at equilibrium. We tried both the FermiNet and Psiformer, and did not find any significant difference in the results, so we show the Psiformer results here (though FermiNet results are included in Table VI). For comparison, in addition to TD-DFT⁵⁷ and MR-CI, we also compare against the PauliNet penalty method¹⁸. For consistency, we show the PauliNet penalty method without variance matching, though the difference is not large. All results are normalized so that the ground state energy at



(a) Energy levels of benzene. The PauliNet energy from Entwistle *et al.*¹⁸ without variance matching is obscured by the legend.

FIG. 6: Excited states of benzene. The NES-VMC results (green and blue) are compared against theoretical best estimates from QUEST^{50,54} alongside TD-DFT-PBE0⁶⁵, CASPT2⁶⁶, DMC with a Slater-Jastrow Ansatz and penalty method¹⁷, and the PauliNet with a penalty method¹⁸. NES-VMC with the Psiformer Ansatz is competitive with state-of-the-art methods. All excitations are $\pi \rightarrow \pi^*$ excitations, and the orbitals involved are visualized in Fig 6b. Complete numerical results are given in Table VII.



(b) The orbitals involved in the excitation of benzene. Top row: π orbitals occupied in the ground state. Bottom row: π^* orbitals occupied in the excited states.

the equilibrium geometry is 0.

Qualitatively, the results from NES-VMC closely match MR-CI. The spurious cusp when the torsion angle is 90° is avoided, and the error in the ground state relative to MR-CI is smaller than for the PauliNet penalty method across torsion angles. The non-parallelity error in the V state relative to MR-CI is lower for our method than the PauliNet penalty method, and our predicted location for the conical intersection (~ 97.5 degrees) is closer to the MR-CI value (~ 96 degrees) than the predicted PauliNet penalty method value (~ 100 degrees). There is a nearly constant shift in the energy of the V state on the order of several tenths of an eV relative to MR-CI, and a shift in the energy of the N state which grows as the pyramidalization angle grows. Increasing the number of excited states and using a different Ansatz did not seem to make a difference. We note that when using the equilibrium geometry for ethylene from QUEST in Sec IIIB as opposed to the geometry from MR-CI, our results agreed with the theoretical best estimates to within chemical accuracy. The overall agreement with experimentally relevant quantities like the location of the conical intersection is in excellent agreement with other highly accurate theoretical studies, and so we are confident that NES-VMC is able to capture the important behavior of this system across the potential energy surface.

E. Benzene

Finally, as a demonstration of the ability of our method to scale to larger systems, we applied NES-VMC with both the FermiNet and Psiformer to benzene. Benzene is a common benchmark for excited state methods for medium-sized molecules, so there is abundant data for us to compare against. For VMC, in addition to the penalty method of Entwistle *et al.*¹⁸, there is also the penalty method of Pathak *et al.*¹⁷, which is used in combination with a traditional Slater-Jastrow Ansatz, and uses a different form of the penalty function which allows for unbiased gradients. On top of VMC results and coupled-cluster-based TBEs from QUEST, we also compare against CASPT2⁶⁶ and TD-DFT with the PBE0 functional⁶⁵. Results are shown in Fig. 6, with complex numerical results in Table VII. For our calculations, we used the same geometry as in QUEST⁵⁰.

As can be seen in Fig 6a, NES-VMC with the Psiformer comes very close to reaching the TBE for all computed states. The FermiNet is not quite as accurate, and struggles with the highest energy $^3B_{2u}$ state. Inspection of the spin magnitude reveals that the highest excited state of the FermiNet converges to a mixture of a triplet and singlet state, which suggests that contamination from the $^1B_{1u}$ state is affecting the performance. The Psiformer is known to be much more accurate for ground state calculations on systems as large as benzene³⁸, so it is not surprising that the Psiformer is also better suited for computing the relative energy between states at this

scale. CASPT2 and TD-DFT methods are less accurate across the board, though this is not surprising as density functional methods are generally less accurate than wavefunction methods, and CASPT2 is generally intermediate in accuracy between DFT and coupled cluster. The penalty method of Entwistle *et al.* in combination with the PauliNet was only applied to the lowest excited state, and even on that, it only reaches CASPT2-level accuracy, even with variance matching (which we do not use in NES-VMC). The penalty method of Pathak *et al.*, however, is much more accurate, generally reaching comparable levels of accuracy to NES-VMC with the Psi-former. We suspect this is due to the unbiased gradients in the method of Pathak *et al.*. Additionally, the results reported in Pathak *et al.* include a diffusion Monte Carlo correction, which we omit, though this only reduces the root mean squared error by ~ 0.1 eV. We note that NES-VMC with a sufficiently expressive Ansatz not only reaches levels of accuracy near coupled cluster, but does so without any free parameters to tune, unlike penalty methods.

To better understand the nature of the excitations computed, we inspected the density matrices of the respective states, similarly to the analysis of the carbon dimer in Sec III C and Fig. 3c. The natural orbitals are well described by the Hartree-Fock orbitals, and so the density matrices in the Hartree-Fock basis are all nearly diagonal. All five excited states for benzene we computed are single excitations from a π to π^* orbital, but interestingly, in the natural orbital picture, they are best described by exciting half an electron from two distinct π_g orbitals into two distinct π_u^* orbitals. These orbitals are visualized in Fig 6b. The ability to easily evaluate and analyze properties of wavefunctions other than just the energy is one of the advantages of explicitly computing the functional form of the wavefunction in VMC. Overall, our results on benzene show that NES-VMC can be usefully applied to larger systems and still produce accurate results, so long as the correct Ansatz is used.

IV. DISCUSSION

We have presented a novel method for calculating excited state properties of quantum systems by variational quantum Monte Carlo (VMC), the Natural Excited States method (NES-VMC). NES-VMC has no free parameters to tune, and allows for unbiased estimation of energies and gradients, by reformulating a state-averaging approach as the problem of finding the ground state of an extended system. In much the same way that sampling from ψ^2 is the natural way to compute ground

state properties by VMC, we believe that NES-VMC is the natural variational principle for computing excited state properties. Additionally, it dovetails well with recent work on neural network Ansätze for many-body systems.

We have demonstrated the effectiveness of NES-VMC on a number of benchmark problems ranging from small atoms and molecules up to the benzene molecule. In all cases, NES-VMC is competitive with theoretical best estimates using coupled cluster methods for estimating energies and oscillator strengths, and can capture the behavior of double excitations and conical intersections. The optimized Ansatz can be used in downstream analyses to characterize the nature of the electronic structure of different excited states. We are confident that NES-VMC is as effective as any other method for computing excited states with QMC, with the added benefit of simplicity and generality.

Neural network Ansätze can be quite computationally expensive, which puts an upper limit on the scale of systems we considered. We believe that recent work on scaling and accelerating neural network Ansätze for many-electron problems⁴¹ can be usefully applied to NES-VMC as well, which could allow these methods to be applied to problems for which no satisfactory solution exists today. While we focused on applications using neural network Ansätze, classic Ansätze like the Slater-Jastrow Ansatz can be scaled to much larger systems^{25,69}. Although our results suggest that more accurate Ansätze are quite important for achieving good performance, we look forward to finding out how well NES-VMC works in conjunction with these classic Ansätze on large problems.

Finally, while our experiments in this paper focused on molecular systems, that is, many-electron problems with open boundary conditions, NES-VMC is fully general and can be applied to *any* quantum Hamiltonian. Excited state calculations with QMC are an important tool for studying nuclear physics⁶, optical band gaps in condensed matter physics^{13,70}, many properties of spin systems, as well as time dynamics and finite temperature phenomena. We are excited to see how NES-VMC can be applied to many of the most challenging open problems in many-body quantum mechanics in the future.

ACKNOWLEDGMENTS

The authors would like to thank Matthew Foulkes, Denis Jacquemin, Michael Bearpark, Aron Cohen and Alex Gaunt for helpful discussions, and James Kirkpatrick, Annette Obika, Ali Eslami and Pushmeet Kohli for support.

* pfau@google.com

¹ J. G. Calvert and J. N. Pitts, *Photochemistry*, Vol. 378

(Wiley New York, 1966).

² D. Polli, P. Altoè, O. Weingart, K. M. Spillane, C. Man-

- zoni, D. Brida, G. Tomasello, G. Orlandi, P. Kukura, R. A. Mathies, *et al.*, *Nature* **467**, 440 (2010).
- ³ C. Kittel and P. McEuen, *Introduction to Solid State Physics* (John Wiley & Sons, 2018).
 - ⁴ C. Chiara, J. Carroll, M. Carpenter, J. Greene, D. Hartley, R. Janssens, G. Lane, J. Marsh, D. Matters, M. Polasik, *et al.*, *Nature* **554**, 216 (2018).
 - ⁵ W. Foulkes, L. Mitas, R. Needs, and G. Rajagopal, *Reviews of Modern Physics* **73**, 33 (2001).
 - ⁶ J. Carlson, S. Gandolfi, F. Pederiva, S. C. Pieper, R. Schiavilla, K. Schmidt, and R. B. Wiringa, *Reviews of Modern Physics* **87**, 1067 (2015).
 - ⁷ G. Carleo and M. Troyer, *Science* **355**, 602 (2017).
 - ⁸ J. Hermann, J. Spencer, K. Choo, A. Mezzacapo, W. Foulkes, D. Pfau, G. Carleo, and F. Noé, *Nature Reviews Chemistry* **7** (2023).
 - ⁹ Y. Kwon, D. Ceperley, and R. M. Martin, *Physical Review B* **48**, 12037 (1993).
 - ¹⁰ M. Bajdich, L. Mitas, L. Wagner, and K. Schmidt, *Physical Review B* **77**, 115112 (2008).
 - ¹¹ S. Sorella, *Physical Review Letters* **80**, 4558 (1998).
 - ¹² J. Toulouse and C. J. Umrigar, *The Journal of Chemical Physics* **126**, 084102 (2007).
 - ¹³ L. Zhao and E. Neuscamman, *Physical Review Letters* **123**, 036402 (2019).
 - ¹⁴ L. Otis and E. Neuscamman, *Wiley Interdisciplinary Reviews: Computational Molecular Science*, e1659 (2023).
 - ¹⁵ K. Choo, G. Carleo, N. Regnault, and T. Neupert, *Physical Review Letters* **121**, 167204 (2018).
 - ¹⁶ P. M. Zimmerman, J. Toulouse, Z. Zhang, C. B. Musgrave, and C. Umrigar, *The Journal of Chemical Physics* **131**, 124103 (2009).
 - ¹⁷ S. Pathak, B. Busemeyer, J. N. Rodrigues, and L. K. Wagner, *The Journal of Chemical Physics* **154**, 034101 (2021).
 - ¹⁸ M. Entwistle, Z. Schätzle, P. A. Erdman, J. Hermann, and F. Noé, *Nature Communications* **14**, 274 (2023).
 - ¹⁹ F. Schautz and C. Filippi, *The Journal of chemical physics* **120**, 10931 (2004).
 - ²⁰ F. Cordova, L. J. Doriol, A. Ipatov, M. E. Casida, C. Filippi, and A. Vela, *The Journal of Chemical Physics* **127** (2007).
 - ²¹ A. Cuzzocrea, A. Scemama, W. J. Briels, S. Moroni, and C. Filippi, *Journal of Chemical Theory and Computation* **16**, 4203 (2020).
 - ²² M. Dash, S. Moroni, C. Filippi, and A. Scemama, *Journal of chemical theory and computation* **17**, 3426 (2021).
 - ²³ J. J. Dorando, J. Hachmann, and G. K. Chan, *The Journal of Chemical Physics* **127** (2007).
 - ²⁴ M. Lewin, *Journal of Mathematical Chemistry* **44**, 967 (2008).
 - ²⁵ C. Filippi, M. Zaccheddu, and F. Buda, *Journal of Chemical Theory and Computation* **5**, 2074 (2009).
 - ²⁶ D. M. Ceperley and B. Bernu, *The Journal of Chemical Physics* **89**, 6316 (1988).
 - ²⁷ M. Nightingale and V. Melik-Alaverdian, *Physical Review Letters* **87**, 043401 (2001).
 - ²⁸ D. Luo and B. K. Clark, *Physical Review Letters* **122**, 226401 (2019).
 - ²⁹ D. Pfau, J. S. Spencer, A. G. Matthews, and W. M. C. Foulkes, *Physical Review Research* **2**, 033429 (2020).
 - ³⁰ J. Hermann, Z. Schätzle, and F. Noé, *Nature Chemistry* **12**, 891 (2020).
 - ³¹ J. Carlson, V. R. Pandharipande, and R. B. Wiringa, *Nuclear Physics A* **424**, 47 (1984).
 - ³² J. E. Sansonetti and W. C. Martin, *Journal of Physical and Chemical Reference Data* **34**, 1559 (2005).
 - ³³ M. Motta and S. Zhang, *Wiley Interdisciplinary Reviews: Computational Molecular Science* **8**, e1364 (2018).
 - ³⁴ Y. Yang and P. Zhao, *Physical Review C* **107**, 034320 (2023).
 - ³⁵ J. Stokes, J. R. Moreno, E. A. Pnevmatikakis, and G. Carleo, *Physical Review B* **102**, 205122 (2020).
 - ³⁶ O. Sharir, Y. Levine, N. Wies, G. Carleo, and A. Shashua, *Physical review letters* **124**, 020503 (2020).
 - ³⁷ L. Gerard, M. Scherbela, P. Marquetand, and P. Grohs, *Advances in Neural Information Processing Systems (NeurIPS)* **35**, 10282 (2022).
 - ³⁸ I. von Glehn, J. S. Spencer, and D. Pfau, *The 11th International Conference on Learning Representations (ICLR)*.
 - ³⁹ N. Gao and S. Günnemann, *arXiv preprint arXiv:2302.04168* (2023).
 - ⁴⁰ G. Pescia, J. Nys, J. Kim, A. Lovato, and G. Carleo, *arXiv preprint arXiv:2305.07240* (2023).
 - ⁴¹ R. Li, H. Ye, D. Jiang, X. Wen, C. Wang, Z. Li, X. Li, D. He, J. Chen, W. Ren, *et al.*, *arXiv preprint arXiv:2307.08214* (2023).
 - ⁴² E. Wigner and F. Seitz, *Physical Review* **46**, 509 (1934).
 - ⁴³ L. Bottou and O. Bousquet, *Advances in Neural Information Processing Systems (NeurIPS)* **20** (2007).
 - ⁴⁴ M. Born and R. Oppenheimer, *Annalen der Physik* **389**, 457 (1927).
 - ⁴⁵ A. Chrayteh, A. Blondel, P.-F. Loos, and D. Jacquemin, *Journal of Chemical Theory and Computation* **17**, 416 (2020).
 - ⁴⁶ M. Vénil, A. Scemama, M. Caffarel, F. Lipparini, M. Boggio-Pasqua, D. Jacquemin, and P.-F. Loos, *Wiley Interdisciplinary Reviews: Computational Molecular Science* **11**, e1517 (2021).
 - ⁴⁷ A. Tanabashi, T. Hirao, T. Amano, and P. Bernath, *The Astrophysical Journal Supplement Series* **169**, 472 (2007).
 - ⁴⁸ P.-F. Loos, M. Boggio-Pasqua, A. Scemama, M. Caffarel, and D. Jacquemin, *Journal of Chemical Theory and Computation* **15**, 1939 (2019).
 - ⁴⁹ P.-F. Loos, A. Scemama, A. Blondel, Y. Garniron, M. Caffarel, and D. Jacquemin, *Journal of Chemical Theory and Computation* **14**, 4360 (2018).
 - ⁵⁰ P.-F. Loos, F. Lipparini, M. Boggio-Pasqua, A. Scemama, and D. Jacquemin, *Journal of Chemical Theory and Computation* **16**, 1711 (2020).
 - ⁵¹ P.-F. Loos, A. Scemama, M. Boggio-Pasqua, and D. Jacquemin, *Journal of Chemical Theory and Computation* **16**, 3720 (2020).
 - ⁵² P.-F. Loos, M. Comin, X. Blase, and D. Jacquemin, *Journal of Chemical Theory and Computation* **17**, 3666 (2021).
 - ⁵³ P.-F. Loos and D. Jacquemin, *The Journal of Physical Chemistry A* **125**, 10174 (2021).
 - ⁵⁴ P.-F. Loos, F. Lipparini, D. A. Matthews, A. Blondel, and D. Jacquemin, *Journal of Chemical Theory and Computation* **18**, 4418 (2022).
 - ⁵⁵ R. Crossley, *Physica Scripta* **1984**, 117 (1984).
 - ⁵⁶ M. Dash, J. Feldt, S. Moroni, A. Scemama, and C. Filippi, *Journal of Chemical Theory and Computation* **15**, 4896 (2019).
 - ⁵⁷ M. Mališ and S. Lubner, *Journal of Chemical Theory and Computation* **16**, 4071 (2020).
 - ⁵⁸ M. Barbatti, J. Paier, and H. Lischka, *The Journal of Chemical Physics* **121**, 11614 (2004).
 - ⁵⁹ J. G. Phillips and S. P. Davis, *The Swan system of the C2*

molecule: the spectrum of the HgH molecule, Vol. 2 (Univ of California Press, 1968).

- ⁶⁰ J. Jiang, H.-Z. Ye, K. Nauta, T. Van Voorhis, T. W. Schmidt, and R. W. Field, *The Journal of Physical Chemistry A* **126**, 3090 (2022).
- ⁶¹ K. Venkataramani, S. Ghetiya, S. Ganesh, U. Joshi, V. K. Agnihotri, and K. S. Baliyan, *Monthly Notices of the Royal Astronomical Society* **463**, 2137 (2016).
- ⁶² S. Shaik, D. Danovich, W. Wu, P. Su, H. S. Rzepa, and P. C. Hiberty, *Nature Chemistry* **4**, 195 (2012).
- ⁶³ E. Ballik and D. Ramsay, *The Astrophysical Journal* **137**, 61 (1963).
- ⁶⁴ E. Ballik and D. Ramsay, *The Astrophysical Journal* **137**, 84 (1963).
- ⁶⁵ C. Adamo, G. E. Scuseria, and V. Barone, *The Journal of chemical physics* **111**, 2889 (1999).
- ⁶⁶ B. O. Roos, K. Andersson, and M. P. Fülcher, *Chemical Physics Letters* **192**, 5 (1992).
- ⁶⁷ A. I. Krylov, C. D. Sherrill, E. F. Byrd, and M. Head-Gordon, *The Journal of Chemical Physics* **109**, 10669 (1998).
- ⁶⁸ M. Barbatti and R. Crespo-Otero, *Density-Functional Methods for Excited States*, 415 (2016).
- ⁶⁹ R. Send, O. Valsson, and C. Filippi, *Journal of Chemical Theory and Computation* **7**, 444 (2011).
- ⁷⁰ R. J. Hunt, M. Szyniszewski, G. I. Prayogo, R. Maezono, and N. D. Drummond, *Physical Review B* **98**, 075122 (2018).
- ⁷¹ J. S. Spencer, D. Pfau, A. Botev, and W. M. C. Foulkes, *arXiv preprint arXiv:2011.07125* (2020).
- ⁷² A. Vaswani, N. Shazeer, N. Parmar, J. Uszkoreit, L. Jones, A. N. Gomez, L. Kaiser, and I. Polosukhin, *Advances in Neural Information Processing Systems (NeurIPS)* **30** (2017).
- ⁷³ J. L. Ba, J. R. Kiros, and G. E. Hinton, *arXiv preprint arXiv:1607.06450* (2016).
- ⁷⁴ K. He, X. Zhang, S. Ren, and J. Sun, in *Proceedings of the IEEE Conference on Computer Vision and Pattern Recognition (CVPR)* (2016) pp. 770–778.
- ⁷⁵ Q. Sun, T. C. Berkelbach, N. S. Blunt, G. H. Booth, S. Guo, Z. Li, J. Liu, J. D. McClain, E. R. Sayfutyarova, S. Sharma, *et al.*, *Wiley Interdisciplinary Reviews: Computational Molecular Science* **8**, e1340 (2018).
- ⁷⁶ S. Fahy, X. Wang, and S. G. Louie, *Physical Review B* **42**, 3503 (1990).
- ⁷⁷ M. C. Bennett, G. Wang, A. Annaberdiyev, C. A. Melton, L. Shulenburg, and L. Mitas, *The Journal of Chemical Physics* **149** (2018).
- ⁷⁸ X. Li, C. Fan, W. Ren, and J. Chen, *Physical Review Research* **4**, 013021 (2022).
- ⁷⁹ P. A. M. Dirac, *Proceedings of the Royal Society A* **123**, 714 (1929).
- ⁸⁰ P.-O. Löwdin, *Physical Review* **97**, 1474 (1955).
- ⁸¹ J. Wang, A. D. Becke, and V. H. Smith, *Journal of Chemical Physics* **102**, 3477 (1995).
- ⁸² D. Lewart, V. Pandharipande, and S. C. Pieper, *Physical Review B* **37**, 4950 (1988).

Appendix A: Derivation of the Local Energy Matrix

Here we give a more detailed derivation of Eq. 9, that the local total energy is the same as the trace of the

local energy matrix. First we write out the effect of the total Hamiltonian on the total Ansatz using the Leibniz definition of the determinant:

$$\hat{\mathcal{H}}\Psi(\mathbf{x}) = \hat{\mathcal{H}} \sum_{\sigma} (-1)^{|\sigma|} \prod_{i=1}^K \psi_{\sigma_i}(\mathbf{x}^i) \quad (\text{A1})$$

$$= \hat{H}_1 \oplus \dots \oplus \hat{H}_K \sum_{\sigma} (-1)^{|\sigma|} \prod_{i=1}^K \psi_{\sigma_i}(\mathbf{x}^i) \quad (\text{A2})$$

$$= \sum_{j=1}^K \sum_{\sigma} (-1)^{|\sigma|} \hat{H} \psi_{\sigma_j}(\mathbf{x}^j) \prod_{i \neq j} \psi_{\sigma_i}(\mathbf{x}^i) \quad (\text{A3})$$

$$= \sum_{j=1}^K \det \begin{pmatrix} \psi_1(\mathbf{x}^1) & \dots & \psi_K(\mathbf{x}^1) \\ \vdots & & \vdots \\ \hat{H} \psi_1(\mathbf{x}^j) & \dots & \hat{H} \psi_K(\mathbf{x}^j) \\ \vdots & & \vdots \\ \psi_1(\mathbf{x}^K) & \dots & \psi_K(\mathbf{x}^K) \end{pmatrix} \quad (\text{A4})$$

where the sum over σ is over all K -permutations. The matrices in the sum in Eq. A4 are rank-one updates to $\Psi(\mathbf{x})$ of the form $\mathbf{e}_j(\hat{H}\Psi_j - \Psi_j)\Psi^{-1}(\mathbf{x})\mathbf{e}_j$ where Ψ_j is the j th row of Ψ and $\hat{H}\Psi_j$ is the row vector with elements $\hat{H}\psi_i(\mathbf{x}^j)$. Plugging this into the matrix determinant lemma yields

$$\hat{\mathcal{H}}\Psi(\mathbf{x}) = \sum_{j=1}^K \det \Psi(\mathbf{x}) \left(1 + (\hat{H}\Psi_j - \Psi_j)\Psi^{-1}(\mathbf{x})\mathbf{e}_j \right) \quad (\text{A5})$$

$$= \sum_{j=1}^K \Psi(\mathbf{x}) \left(1 + \hat{H}\Psi_j\Psi^{-1}(\mathbf{x})\mathbf{e}_j - \Psi_j\Psi^{-1}(\mathbf{x})\mathbf{e}_j \right) \quad (\text{A6})$$

$$= \sum_{j=1}^K \Psi(\mathbf{x}) \left(1 + \hat{H}\Psi_j\Psi^{-1}(\mathbf{x})\mathbf{e}_j - \mathbf{e}_j^T \mathbf{e}_j \right) \quad (\text{A7})$$

$$= \sum_{j=1}^K \Psi(\mathbf{x}) \left(\hat{H}\Psi_j\Psi^{-1}(\mathbf{x})\mathbf{e}_j \right) \quad (\text{A8})$$

And plugging this into the expression for the local total energy yields

$$\Psi(\mathbf{x})^{-1} \hat{\mathcal{H}}\Psi(\mathbf{x}) = \sum_{j=1}^K \hat{H}\Psi_j\Psi^{-1}(\mathbf{x})\mathbf{e}_j \quad (\text{A9})$$

$$= \text{Tr} \left[\hat{H}\Psi(\mathbf{x})\Psi^{-1}(\mathbf{x}) \right] \quad (\text{A10})$$

$$= \text{Tr} \left[\Psi^{-1}(\mathbf{x})\hat{H}\Psi(\mathbf{x}) \right] \quad (\text{A11})$$

The rest of Eq 9 follows from the linearity of expectations.

Appendix B: Experimental Details

Here we go into more depth about the numerical details of implementation, as well as the specific hyperparame-

ters used for different experiments.

1. The FermiNet and Psiformer Ansätze

The exact form of the FermiNet and Psiformer Ansätze are described in more detail in their respective papers^{29,38,71}. We give a brief summary here.

Both Ansätze take electron positions $\mathbf{r}_1, \dots, \mathbf{r}_N$ as inputs, and assume that the spins are fixed, so that the first N_α electrons are spin up, while the last $N_\beta = N - N_\alpha$ electrons are spin down. Where relevant, we will add a superscript of α or β to \mathbf{r}_i to indicate the spin. For both the FermiNet and Psiformer, the vector differences between atoms and ions $\mathbf{r}_i - \mathbf{R}_I$ and scalar distances $|\mathbf{r}_i - \mathbf{R}_I|$ are concatenated as input features. Additionally in the FermiNet, the differences $\mathbf{r}_i - \mathbf{r}_j$ and distances $|\mathbf{r}_i - \mathbf{r}_j|$ between pairs of electrons form the input to the two-electron stream of the network.

In both the FermiNet and Psiformer, these inputs are propagated through multiple layers of nonlinear computation. In the Psiformer, each layer consists of a standard self-attention layer⁷² with layer normalization⁷³ and a residual connection⁷⁴ followed by parallel linear-nonlinear layers with a hyperbolic tangent nonlinearity. In the FermiNet, the two-electron stream consists entirely of parallel linear-nonlinear layers with hyperbolic tangent nonlinearities and residual connections. The one-electron stream integrates information from the two-electron stream as well as between different activations in the one-electron stream. If $\mathbf{h}_i^{\ell\alpha}$ is the activation vector at layer ℓ for electron i of spin α in the one-electron stream and $\mathbf{h}_{ij}^{\ell\alpha\beta}$ is the activation vector for electrons i and j of spin α and β in the two electron stream, then

$$\begin{aligned} \mathbf{f}_i^{\ell\alpha} &= \left(\mathbf{h}_i^{\ell\alpha}, \frac{1}{n^\uparrow} \sum_{j=1}^{n^\uparrow} \mathbf{h}_j^{\ell\uparrow}, \frac{1}{n^\downarrow} \sum_{j=1}^{n^\downarrow} \mathbf{h}_j^{\ell\downarrow}, \right. \\ &\quad \left. \frac{1}{n^\uparrow} \sum_{j=1}^{n^\uparrow} \mathbf{h}_{ij}^{\ell\alpha\uparrow}, \frac{1}{n^\downarrow} \sum_{j=1}^{n^\downarrow} \mathbf{h}_{ij}^{\ell\alpha\downarrow} \right) \\ \mathbf{h}_i^{(\ell+1)\alpha} &= \tanh(\mathbf{W}^\ell \mathbf{f}_i^{\ell\alpha} + \mathbf{b}^\ell) + \mathbf{h}_i^{\ell\alpha} \end{aligned} \quad (\text{B1})$$

gives the activation at the next layer.

Following the sequence of repeated nonlinear layers, the final activations $\mathbf{h}_i^{L\alpha}$ are linearly projected to a set of orbitals, one spin up and one spin down, and multiplied by an exponentially-decaying envelope which enforces the boundary condition that the wavefunction should decay to zero at long range, described in more detail below in Sec. B 2. The form of these orbitals can be written as:

$$\phi_i^{k\alpha}(\mathbf{r}_j^\alpha; \{\mathbf{r}_{/j}^\alpha\}; \{\mathbf{r}^{\bar{\alpha}}\}) = (\mathbf{w}_i^{k\alpha} \cdot \mathbf{h}_j^{L\alpha} + g_i^{k\alpha}) e_i^{k\alpha}(\mathbf{r}_j^\alpha) \quad (\text{B2})$$

Finally, for the Psiformer, a multiplicative Jastrow factor $\exp(\mathcal{J}_\theta(\mathbf{r}_1^\uparrow, \dots, \mathbf{r}_N^\downarrow))$ is applied after the determinant

to capture the correct behavior at the electron-electron cusps, due to the lack of two-electron inputs to the neural network part of the Ansatz. A simple two-parameter Jastrow factor seems to suffice:

$$\begin{aligned} \mathcal{J}_\theta(\mathbf{r}_1^\uparrow, \dots, \mathbf{r}_N^\downarrow) &= \sum_{i < j; \alpha = \beta} -\frac{1}{4} \frac{\alpha_{\text{par}}^2}{\alpha_{\text{par}} + |\mathbf{r}_i^\alpha - \mathbf{r}_j^\beta|} + \\ &\quad \sum_{i, j; \alpha \neq \beta} -\frac{1}{2} \frac{\alpha_{\text{anti}}^2}{\alpha_{\text{anti}} + |\mathbf{r}_i^\alpha - \mathbf{r}_j^\beta|} \end{aligned} \quad (\text{B3})$$

2. Bottleneck Envelope

For the experiments with benzene, the memory overhead of the default FermiNet and Psiformer became prohibitive, largely due to the cost of the multiplicative envelope which is used to enforce open boundary conditions. For both the FermiNet and Psiformer, each orbital $\phi_j^{k\alpha}(\mathbf{r}_i^\alpha; \{\mathbf{r}_{/i}^\alpha\}, \{\mathbf{r}^{\bar{\alpha}}\})$ included a multiplicative envelope of the form:

$$e_j^{k\alpha}(\mathbf{r}_i^\alpha) = \sum_I \pi_{jI}^{k\alpha} \exp(\sigma_{jI}^{k\alpha} |\mathbf{r}_i^\alpha - \mathbf{R}_I|) \quad (\text{B4})$$

where i indexes electrons, I indexes atomic nuclei, $\alpha \in \{\uparrow, \downarrow\}$ indexes spin, j indexes different orbitals in a determinant and k indexes different determinants. Because the number of orbitals scales linearly with the number of electrons *and* excited states, this becomes prohibitively large for large molecules with many excited states. Instead, we fix the number of distinct envelopes, and for each orbital we take a weighted sum of these envelopes:

$$e_j^{k\alpha}(\mathbf{r}_i^\alpha) = \sum_\ell w_{j\ell}^{k\alpha} \sum_I \pi_{\ell I}^\alpha \exp(\sigma_{\ell I}^\alpha |\mathbf{r}_i^\alpha - \mathbf{R}_I|) \quad (\text{B5})$$

This reduces the memory overhead when computing the sum over I significantly. In our experiments, we used $|\ell| = 32$, which is far lower than $|k||j| = 336$ for benzene (21 electrons of each spin and 16 determinants). We refer to this as the *bottleneck* envelope, as it can be seen as projecting the envelopes into a lower dimension space and then back into the space of orbitals. Although we did not have any numerical difficulties using the bottleneck envelope for benzene, we did find on some systems that there were occasional numerical stability issues, and so we only used the bottleneck envelope for the very largest systems we investigated in this paper.

3. Pretraining

If the different states are not linearly independent at initialization, then the total Ansatz will be identically zero and the local energy will be undefined. To avoid

this pathological initialization, we pretrain the single-state Ansätze to be linearly independent. In the original FermiNet paper²⁹, the individual orbitals were pretrained to match Hartree-Fock orbitals computed by PySCF⁷⁵. For excited states, we need to construct k different orthogonal Slater determinants. We compute all the single and double excitations of the Hartree-Fock solution and order them by energy, and pretrain the single-state Ansätze to match the Slater determinants of the k lowest excitations. We also use a cc-pVDZ basis set rather than STO-6G to guarantee a sufficient number of single and double excitations. While the excitations found by Hartree-Fock do not necessarily correspond to the true lowest excitations, we only need pretraining to find a decent low-energy non-degenerate starting point, and the optimization will usually quickly find the true lowest energy states. We did occasionally see sudden drops in energy during optimization, which may be due to certain states transitioning away from the state they were initialized to towards states with lower energy, but these drops usually occurred in the first 10-20% of optimization.

4. Numerical Stability

Computation of the local energy becomes numerically unstable at nodes (i.e. when the Ansatz is zero). For variational Monte Carlo calculation of ground states, because walkers are sampled from ψ^2 , it is vanishingly unlikely that a walker will be found close enough to a node that the local energy becomes undefined. However, in natural excited states VMC, the walkers are sampled from $\Psi^2 = \det(\mathbf{\Psi})^2$, so even if Ψ^2 is nonzero, some of the entries $\psi_i(\mathbf{x}^j)$ in the matrix $\mathbf{\Psi}$ might be zero up to numerical precision. To avoid this, we introduce a number of heuristics to stabilize optimization. First, if any entries of $\mathbf{\Psi}$ are zero, we run additional steps of MCMC (up to 10 times per iteration, to avoid an infinite loop). Secondly, if the local energy of any of the walkers is undefined, we remove that walker from the computation of energies and gradients in that step. Lastly, if the gradient still has undefined values, that iteration of optimization is skipped. If more than 100 iterations are skipped in a row, the optimization fails, but we did not find that this happened in any of our experiments. Out of all these heuristics, only the last should really be necessary, as it is more general than the first two.

When calculating the matrices $\mathbf{\Psi}$ and $\hat{O}\mathbf{\Psi}$, we always compute the values of $\psi_i(\mathbf{x}^j)$ and the local operator $O_L^i(\mathbf{x}^j) = \psi_i^{-1}(\mathbf{x}^j)\hat{O}\psi_i(\mathbf{x}^j)$ in the log domain, then subtract the maximum value of $\log\psi_i(\mathbf{x}^j)$ over i and j from the values of both $\log\psi_i(\mathbf{x}^j)$ and $O_L^i(\mathbf{x}^j) + \log\psi_i(\mathbf{x}^j)$ before converting from the log domain to real domain. This avoids issues with numerical underflow or overflow that can occur when computing ψ and $\hat{O}\psi$ directly in the real domain.

System	Ansatz	Pretraining	Blocks/set	Training
Atoms (Sec. III A)	Both	10k	1	200k
Osc. (Sec. III B)	Both	10k	1	200k
C ₂ (Sec. III C)	Psiformer	100k	1	100k
Ethylene (Sec. III D)	Both	10k	1	100k
Benzene (Sec. III E)	FermiNet	100k	4	200k
Benzene (Sec. III E)	Psiformer	100k	4	100k

TABLE I: Settings used for different experiments

5. Pseudopotentials

For molecules with heavier atoms in Sec. III B such as HCl, thioformaldehyde and silylidene, we replaced the core electrons of second-row atoms ($Z = 11 \dots 18$) with a pseudopotential, or effective core potential. We found that this generally led to more accurate results than all-electron calculations, possibly because the energy scale of the core electrons is far greater than the valence electrons for heavier atoms. We followed the general approach for VMC of approximating the core electrons by a non-local one-electron potential⁷⁶, specifically adapting the correlation-consistent effective core potential (ccECP)⁷⁷ from PySCF. A similar approach has been demonstrated with neural network Ansätze to be effective at modeling transition metals⁷⁸.

6. Hyperparameters

For all experiments, we stayed close to the default hyperparameters used in the original papers on the FermiNet^{29,71} and Psiformer³⁸. For all experiments, we used neural network Ansätze with 16 dense determinants, 4 layers and 256 units per layer in the one-electrons stream. For the FermiNet we used 32 units per layer in the two-electron stream, and for the Psiformer we used 4 self-attention heads with 64 units per head, and layer normalization. We follow the gradient scaling from the Psiformer paper, and hence use a learning rate of 0.05. For some larger systems, we increased the number of pretraining steps from 10,000 to 100,000, in line with previous results suggesting that this improved overall accuracy³⁸. While we did not find this made a significant difference, we include details for completeness. We also found that *relative* energies were almost always well converged after 100,000 iterations, so for some larger systems we stopped training then, rather than for the full 200,000 iterations recommended for optimal absolute energies. In each MCMC step, electrons were sampled in blocks rather than one at a time or all simultaneously, as described in the Psiformer paper. Each electron set was treated as at least one block, and for some larger systems, each electron set was further subdivided into multiple blocks. A summary of the different settings used for different experiments is given in Table I.

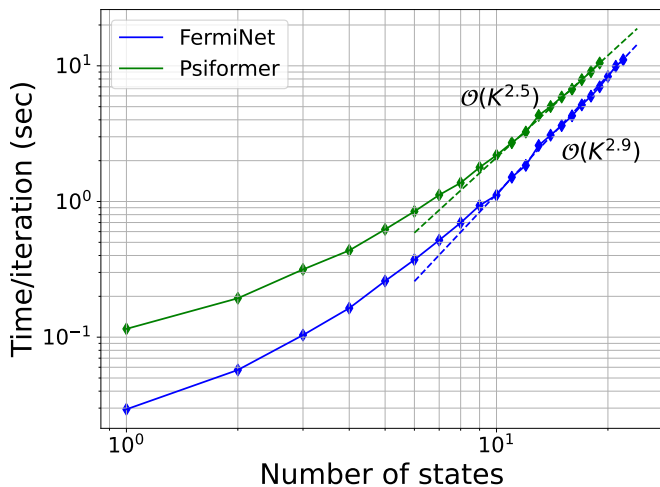


FIG. 7: Time per iteration of NES-VMC optimization on the neon atom on one A100 GPU with a batch size of 64 as a function of the number of excited states. The dashed lines illustrate the sub-cubic scaling for different Ansätze.

7. Time Complexity

In theory, the asymptotic scaling of the NES-VMC optimization as the number of excited states grows is dominated by the calculation of the determinant when evaluating $\Psi = \det(\Psi)$. This scales as $\mathcal{O}(K^3)$ for a single forward evaluation, and $\mathcal{O}(K^4)$ for evaluating the total local energy. However in practice, the computation of the determinant is relatively cheap at the scales investigated in this paper, up to $K = 10$, and the scaling is dominated by the cost of computing the matrix of local energies needed for $\hat{H}\Psi$. Thus a quadratic scaling more accurately reflects the empirical behavior of most experiments in this paper.

In Fig 7, we evaluate the empirical scaling with number of states of NES-VMC applied to the neon atom. All calculations were done with a batch size of 64 on a single A100 GPU, which is much smaller scale than the experiments elsewhere in the paper, which allowed us to investigate scaling for larger K without having to worry about accuracy. It can be seen that for both the FermiNet and Psiformer, the asymptotic time complexity seems to be slightly below cubic, but this scaling does not dominate until $K > 10$. While this may seem costly, it is worth noting that state-of-the-art eigensolvers for finite matrices such as the Lanczos method scale cubically with the number of eigenvalues. When $K < 10$, the roughly quadratic scaling of NES-VMC is comparable to penalty methods, which still require explicit computation of the overlap matrix. We believe that NES-VMC is most appropriate when the number of desired states is relatively small, and the asymptotic scaling is near the optimal scaling for any exact excited states method.

8. Variance Estimation

Because the energies of individual states are not computed directly, the estimation of the variance of the energy for different states must be treated with some care. In addition to computing the expected value of the local energy matrix \mathbf{E}_L , we compute the covariance matrix of the vectorized local energy matrix $\Sigma_{\mathbf{E}_L} = \text{Cov}[\text{vec}(\mathbf{E}_L)] \in \mathbb{R}^{K^2 \times K^2}$. Then after diagonalizing the energy matrix $\mathbb{E}[\mathbf{E}_L] = \mathbf{U}\mathbf{\Lambda}\mathbf{U}^{-1}$, we can transform the covariance to give the covariance of $\mathbf{\Lambda}$ as $\Sigma_{\mathbf{\Lambda}} = (\mathbf{U}^{-1} \otimes \mathbf{U}^T) \Sigma_{\mathbf{E}_L} (\mathbf{U}^{-1} \otimes \mathbf{U}^T)^T$, since $\mathbf{\Lambda} = \mathbf{U}^{-1}\mathbb{E}[\mathbf{E}_L]\mathbf{U}$ can be expressed in vectorized form as $\text{vec}(\mathbf{\Lambda}) = (\mathbf{U}^{-1} \otimes \mathbf{U}^T) \text{vec}(\mathbb{E}[\mathbf{E}_L])$. The diagonal of $\Sigma_{\mathbf{\Lambda}}$ gives the marginal variance of each element of $\text{vec}(\mathbf{\Lambda})$, and reshaping the diagonal as a $K \times K$ matrix, the diagonal of *this* matrix gives the variance of the individual energies of each state. A similar procedure can be used to estimate the uncertainty in other observables.

Appendix C: Observables

As described in Sec. II, observables can be evaluated by computing the matrix $\mathbb{E}_{\Psi^2} [\Psi^{-1} \hat{\mathcal{O}} \Psi]$ and then separating the different states based on the eigenvectors of the energy matrix $\mathbb{E}_{\Psi^2} [\Psi^{-1} \hat{H} \Psi]$. This applies to off-diagonal observables $\langle \psi_i \hat{\mathcal{O}} \psi_j \rangle$ as well, with some additional effort. The exact computational details of the observables considered in this paper – the spin magnitude \mathcal{S}^2 , the density matrix and the dipole moment – require some additional elaboration, which we provide here.

1. Spin Magnitude

In first quantization, the total spin magnitude operator $\hat{\mathcal{S}}^2$ is defined as^{79–81}:

$$\hat{\mathcal{S}}^2 = -\frac{N(N-4)}{4} + \sum_{i < j} \hat{P}_{ij} \quad (\text{C1})$$

where \hat{P}_{ij} is the operator which swaps the spins of particles i and j . In all our experiments, the particles were spin-assigned, so the exact number of α and β electrons is known. The expected value of $\hat{\mathcal{S}}^2$ can be evaluated by Monte Carlo for a single state as:

$$\langle \hat{\mathcal{S}}^2 \rangle = -\frac{N_\alpha - N_\beta}{4} (N_\alpha - N_\beta + 2) + N_\beta - \mathbb{E}_{\psi^2} \left[\sum_{\substack{i=1 \dots N_\alpha \\ j=N_\alpha+1 \dots N}} \frac{\psi(\dots, \sigma_i \mathbf{r}_j, \dots, \sigma_j \mathbf{r}_i, \dots)}{\psi(\dots, \sigma_i \mathbf{r}_i, \dots, \sigma_j \mathbf{r}_j, \dots)} \right] \quad (\text{C2})$$

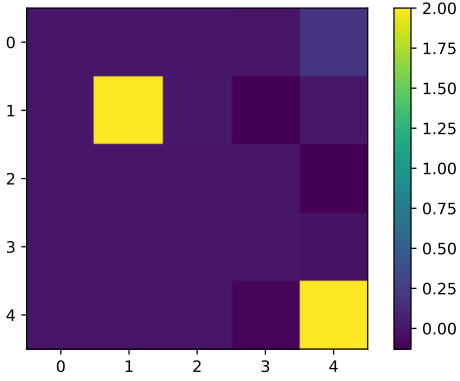


FIG. 8: Matrix of $\langle \hat{S}^2 \rangle$ values for the first 5 excited states of ethylene at equilibrium geometry. Two triplet states can clearly be identified from the diagonal. The off-diagonal terms are all near zero.

where $\sigma\mathbf{r}$ denotes a particle state with the spin σ and position \mathbf{r} . Note that in Eq C2, we swap the particle positions rather than spins, and add a minus sign to the expectation. This makes the implementation simpler for spin-assigned wavefunctions where the first N_α inputs are assumed to have spin α .

To compute this for all excited states, we compute the matrices $\hat{S}^2\Psi(\mathbf{x})$ and $\Psi(\mathbf{x})$, first in the log domain, then subtract off the largest value of $\log\psi_i(\mathbf{x}^j)$ from both matrices for numerical stability, then accumulate the expectation $\mathbb{E}_{\Psi^2}[\Psi^{-1}\hat{S}^2\Psi]$ and finally demixing the states $\mathbf{U}^{-1}\mathbb{E}_{\Psi^2}[\Psi^{-1}\hat{S}^2\Psi]\mathbf{U}$ where \mathbf{U} are the eigenvectors of the energy matrix. Since \hat{S}^2 and \hat{H} commute, the demixed matrix should be diagonal, and we do not need to worry about correcting for the nonidentifiability of Σ . An example result for ethylene is shown in Fig. 8.

2. Density Matrices and Natural Orbitals

The one-electron reduced density matrix is defined as

$$\Gamma(\mathbf{x}_1; \mathbf{x}'_1) = \int d\mathbf{x}_2 \dots d\mathbf{x}_N \psi(\mathbf{x}_1, \mathbf{x}_2, \dots, \mathbf{x}_N) \psi(\mathbf{x}'_1, \mathbf{x}_2, \dots, \mathbf{x}_N) \quad (\text{C3})$$

The eigenfunctions of this operator are the *natural orbitals*, which play a role similar to marginal distributions for probability densities, and it is common to use natural orbitals as a way to analyze the qualitative nature of different Ansätze⁸². For a single Slater determinant wavefunction, the natural orbitals are equal to the true orbitals, up to linear combination. To work with the density matrix in a computationally tractable manner, we can project it into an orthogonal basis set

$\phi_1(\mathbf{x}), \dots, \phi_M(\mathbf{x})$. Elements of this projected density matrix Γ_{ij} are given by

$$\Gamma_{ij} = \int d\mathbf{x}_1 d\mathbf{x}'_1 \phi_i(\mathbf{x}_1) \phi_j(\mathbf{x}'_1) \Gamma(\mathbf{x}_1; \mathbf{x}'_1) \quad (\text{C4})$$

which can be rewritten as the expectation of an observable:

$$\Gamma_{ij} = \langle \hat{\Gamma}_{ij} \rangle \quad (\text{C5})$$

$$\hat{\Gamma}_{ij}(\mathbf{x}; \mathbf{x}') = \phi_i(\mathbf{x}_1) \phi_j(\mathbf{x}'_1) \prod_{k=2}^N \delta(\mathbf{x}_k - \mathbf{x}'_k) \quad (\text{C6})$$

Evaluating this observable by the formula outlined in Sec. II takes some care, as $\hat{\Gamma}_{ij}$ is a nonlocal operator. This means that Monte Carlo estimation of $\hat{\Gamma}_{ij}\Psi$ must be done by integrating over values of \mathbf{x}'_1 as well as $\mathbf{x}_1, \dots, \mathbf{x}_N$. In the case of a single state, a Monte Carlo estimator for Γ_{ij} is given by

$$\langle \hat{\Gamma}_{ij} \rangle = \mathbb{E}_{\mathbf{x} \sim \psi^2, \mathbf{x}'_1 \sim \rho} \left[\frac{\phi_i(\mathbf{x}_1) \phi_j(\mathbf{x}'_1) \psi(\mathbf{x}'_1, \mathbf{x}_2, \dots)}{\rho(\mathbf{x}'_1) \psi(\mathbf{x}_1, \mathbf{x}_2, \dots)} \right] \quad (\text{C7})$$

where ρ is an arbitrary probability distribution over single-particle states. While any ρ can work in theory, a choice of ρ which more closely matches the electron density will give an estimator with lower variance.

In the case of multiple excited states, we calculate not a single density matrix but an entire rank-4 tensor in $\mathbb{R}^{M \times M \times K \times K}$ over both basis set elements and excited states. We sample K sets of N particles $\mathbf{x}_1^1, \dots, \mathbf{x}_N^K$ from Ψ^2 as with local observables, but additionally sample K particles $x_1^1, \dots, x_1^K \sim \rho$ i.i.d. The matrix Ψ is computed as in the local observable case, but calculating $\hat{\Gamma}_{ij}\Psi \in \mathbb{R}^{K \times K}$ is more complicated. For the excited state k and particle set ℓ , the appropriate element of $\hat{\Gamma}_{ij}\Psi$ is given by:

$$\hat{\Gamma}_{ij}\Psi_{k\ell} = \phi_i(\mathbf{x}_1^\ell) \phi_j(\mathbf{x}_1^{\ell'}) \rho^{-1}(\mathbf{x}_1^{\ell'}) \psi^k(\mathbf{x}_1^{\ell'}, \mathbf{x}_2^\ell, \dots, \mathbf{x}_N^\ell) \quad (\text{C8})$$

Finally, as with all other observables, we must unmix the accumulated $\mathbb{E}[\Psi^{-1}\hat{\Gamma}_{ij}\Psi]$ by the eigenvectors of the energy matrix. The diagonals of the demixed matrices can then be assembled into density matrices Γ_{ij}^k for each state k , and then *these* can be diagonalized to recover natural orbitals.

In all experiments in the paper, we used the Hartree-Fock orbitals as computed by PySCF⁷⁵ in the def2-TZVPD basis set as the orthogonal basis set elements ϕ_i , and used the Hartree-Fock electron density $\rho(\mathbf{x}_1) = \frac{1}{N} \sum_{i=1}^N \phi_i^2(\mathbf{x}_1)$ as the sampling distribution for \mathbf{x}'_1 . In practice, we were interested in the natural orbitals for different spin electrons. This meant we would run unrestricted Hartree-Fock, and compute the density matrices twice, once with the α -electron orbitals and once with the β -electron orbitals. In the latter case, we had to be sure to substitute \mathbf{x}'_1 for a β electron rather than an α electron in the spin-assigned wavefunction.

3. Off-Diagonal Expectations and Dipole Moments

For \hat{S}^2 and $\hat{\Gamma}_{ij}$, we primarily care about the expectations for single states $\langle \psi_i \hat{O} \psi_i \rangle$. For computing oscillator strengths, we must work out the transition dipole moments, which are defined as expectations between different states $\langle \psi_i \hat{O} \psi_j \rangle$. The oscillator strength between states i and j is a dimensionless quantity defined as

$$f_{ij} = \frac{2}{3} \frac{m}{\hbar^2} (E_i - E_j) \sum_{k \in x, y, z} \langle \psi_i q \hat{r}_k \psi_j \rangle^2 \quad (\text{C9})$$

where m is the particle mass and q is the particle charge, both 1 for electrons in atomic units (as is \hbar) and \hat{r}_x , \hat{r}_y and \hat{r}_z are the operators for the sum of the x, y and z positions of all particles in the system. The transition dipole moment \mathbf{d}^{ij} is the 3-vector made up of these off-diagonal expectations $d_k^{ij} = \langle \psi_i q \hat{r}_k \psi_j \rangle$. The Monte Carlo estimator for each element of the transition dipole

moment vector is quite simple: $\hat{r}_k \Psi = \mathbf{R}_k \Psi$ where \mathbf{R}_k is a diagonal matrix with $\sum_i r_{ik}^\ell$ in the ℓ th diagonal – that is, the sum of the position along coordinate k taken over all electrons in particle set ℓ . Note that we have dropped the charge, as we are in atomic units. The only additional wrinkle in comparison to other observables we have discussed is that, after demixing the accumulated matrix by the eigenvectors of the energy matrix $\mathbf{\Delta}_k = \mathbf{U}^{-1} \mathbb{E}_{\Psi^2} [\Psi^{-1} \mathbf{R}_k \Psi] \mathbf{U}$, we must multiply this matrix elementwise by its transpose $\mathbf{\Delta}_k^2 = \mathbf{\Delta}_k \circ \mathbf{\Delta}_k^T$ to cancel out a nonidentifiable scaling term. This gives the off-diagonal expectations squared $\langle \psi_i \hat{r}_k \psi_j \rangle^2$, which is precisely the term needed for the oscillator strength.

Appendix D: Numerical Results

Here we provide tables of numbers corresponding to the figures in the main paper.

System	NES-VMC Energy (Ha)			NES-VMC ΔE (Ha)			Config.	Term	Expt.	Error (mHa)		
	FermiNet		Psiformer	FermiNet		Psiformer				FermiNet		Psiformer
	$k = 5$	$k = 10$	$k = 10$	$k = 5$	$k = 10$	$k = 10$				$k = 5$	$k = 10$	$k = 10$
Li	-7.478059(3)	-7.478059(3)	-7.478065(3)	-	-	-	$2s$	2S	-	-	-	-
	-7.410157(5)	-7.410154343(6)	-7.410156(3)	0.067902(6)	0.067904(3)	0.067908(5)	$2p$	$^2P^\circ$	0.067907	-0.005(6)	-0.002(3)	0.001(5)
	-7.4101481(2)	-7.410154343(6)	-7.410147(4)	0.067911(3)	0.067904(3)	0.067917(5)	"	"	0.067907	0.004(3)	-0.002(3)	0.010(5)
	-7.4101481(2)	-7.410145(3)	-7.410144(5)	0.067911(3)	0.067914(4)	0.067921(6)	"	"	0.067907	0.004(3)	0.007(4)	0.014(6)
	-7.35379(1)	-7.354037(5)	-7.354095(5)	0.12427(1)	0.124022(6)	0.123970(6)	$3s$	2S	0.123960	0.31(1)	0.062(6)	0.010(6)
	-7.337074(9)	-7.337147(5)	-7.337136(5)	-	0.14098(1)	0.140918(6)	$3p$	$^2P^\circ$	0.140907	-	0.08(1)	0.010(6)
	-7.3370438(7)	-7.337136(5)	-7.337136(5)	-	0.141015(3)	0.140928(6)	"	"	0.140907	-	0.108(3)	0.021(6)
	-7.3370438(7)	-7.337130(4)	-7.337130(4)	-	0.141015(3)	0.140935(5)	"	"	0.140907	-	0.108(3)	0.028(5)
	-7.335469(6)	-7.335513(4)	-7.335513(4)	-	0.142590(7)	0.142552(5)	$3d$	2D	0.142536	-	0.054(7)	0.016(5)
	-7.335454(7)	-7.335500(4)	-7.335500(4)	-	0.142605(8)	0.142565(5)	"	"	0.142536	-	0.069(8)	0.029(5)
Be	-14.667340(8)	-14.667315(7)	-14.667329(6)	-	-	-	$2s^2$	1S	-	-	-	-
	-14.56723(1)	-14.567224(8)	-14.56723(1)	0.10011(1)	0.10009(1)	0.10010(1)	$2s2p$	$^3P^\circ$	0.100149	-0.04(1)	-0.06(1)	-0.05(1)
	-14.5672150(1)	-14.567214(1)	-14.567219(1)	0.100125(8)	0.100101(7)	0.100110(6)	"	"	0.100149	-0.024(8)	-0.048(7)	-0.039(6)
	-14.5672150(1)	-14.567214(1)	-14.567219(1)	0.100125(8)	0.100101(7)	0.100110(6)	"	"	0.100149	-0.024(8)	-0.048(7)	-0.039(6)
	-14.473414(9)	-14.4734154(7)	-14.47344(1)	0.19393(1)	0.193899(7)	0.19389(1)	$2s2p$	$^1P^\circ$	0.193942	-0.02(1)	-0.043(7)	-0.05(1)
	-14.473414(9)	-14.4734154(7)	-14.4734211(8)	-	0.193899(7)	0.193908(6)	"	"	0.193942	-	-0.043(7)	-0.034(6)
	-14.473414(9)	-14.473405(8)	-14.4734211(8)	-	0.19391(1)	0.193908(6)	"	"	0.193942	-	-0.03(1)	-0.034(6)
	-14.42992(2)	-14.430005(9)	-14.430005(9)	-	0.23739(2)	0.23732(1)	$2s3s$	3S	0.237298	-	0.10(2)	0.03(1)
	-14.41773(2)	-14.41810(1)	-14.41810(1)	-	0.24958(2)	0.24923(1)	$2s3s$	1S	0.249128	-	0.45(2)	0.10(1)
	-14.40802(1)	-14.40815(1)	-14.40815(1)	-	0.25929(1)	0.25917(1)	$2p^2$	1D	0.259175	-	0.12(1)	-0.00(1)
B	-24.65383(1)	-24.6537704(5)	-24.65383(1)	-	-	-	$2s^22p$	$^2P^\circ$	-	-	-	-
	-24.653805(1)	-24.6537704(5)	-24.653811(1)	0.00002(1)	0.000000(7)	0.00002(1)	"	"	0.000000	0.02(1)	0.0000(7)	0.02(1)
	-24.653805(1)	-24.65374(1)	-24.653811(1)	0.00002(1)	0.00003(1)	0.00002(1)	"	"	0.000000	0.02(1)	0.03(1)	0.02(1)
	-24.52198(1)	-24.5219383(1)	-24.521969(7)	0.13185(1)	0.1318321(5)	0.13186(1)	$2s2p^2$	4P	0.131528	0.32(1)	0.3038(5)	0.33(1)
	-24.52196(1)	-24.5219383(1)	-24.521969(7)	0.13187(1)	0.1318321(5)	0.13186(1)	"	"	0.131528	0.34(1)	0.3038(5)	0.33(1)
	-24.52196(1)	-24.52190(1)	-24.52196(3)	-	0.13187(1)	0.13187(3)	"	"	0.131528	-	0.35(1)	0.34(3)
	-24.47114(2)	-24.47114(2)	-24.47134(1)	-	0.18263(2)	0.18249(1)	$2s^23s$	2S	0.182388	-	0.24(2)	0.10(1)
	-24.435720(2)	-24.435757(3)	-24.435757(3)	-	0.218050(2)	0.21807(1)	$2s2p^2$	2D	0.218006	-	0.044(2)	0.07(1)
	-24.435720(2)	-24.435757(3)	-24.435757(3)	-	0.218050(2)	0.21807(1)	"	"	0.218006	-	0.044(2)	0.07(1)
	-24.43547(3)	-24.43219(1)	-24.43219(1)	-	0.21830(3)	0.22164(2)	"	"	0.218006	-	0.29(3)	3.63(2)*
C	-37.844746(3)	-37.84478(2)	-37.84478(1)	-	-	-	$2s^22p^2$	3P	-	-	-	-
	-37.844746(3)	-37.84472(2)	-37.84473(2)	0.000000(5)	0.00007(3)	0.00004(2)	"	"	0.000000	0.000(5)	0.07(3)	0.04(2)
	-37.84464(2)	-37.84468(2)	-37.84471(1)	0.00011(2)	0.00011(3)	0.00006(2)	"	"	0.000000	0.11(2)	0.11(3)	0.06(2)
	-37.79839(2)	-37.79843(2)	-37.798439(1)	0.04635(2)	0.04636(3)	0.04634(1)	$2s^2p^2$	1D	0.046306	0.05(2)	0.05(3)	0.03(1)
	-37.79833(2)	-37.79840(5)	-37.798439(1)	0.04641(2)	0.04638(5)	0.04634(1)	"	"	0.046306	0.11(2)	0.08(5)	0.03(1)
	-37.79839(2)	-37.79839(5)	-37.798431(3)	-	0.04639(5)	0.04634(1)	"	"	0.046306	-	0.09(5)	0.04(1)
	-37.79834(2)	-37.79834(2)	-37.798431(3)	-	0.04644(2)	0.04634(1)	"	"	0.046306	-	0.14(2)	0.04(1)
	-37.79827(2)	-37.79836(1)	-37.79836(1)	-	0.04651(2)	0.04642(2)	"	"	0.046306	-	0.21(2)	0.11(2)
	-37.74617(1)	-37.74623(1)	-37.74623(1)	-	0.09861(2)	0.09855(2)	$2s^2p^2$	1S	0.098501	-	0.11(2)	0.04(2)
	-37.69158(2)	-37.69160(1)	-37.69160(1)	-	0.15321(2)	0.15318(2)	$2s2p^3$	$^5S^\circ$	0.153574	-	-0.37(2)	-0.40(2)
N	-54.58890(2)	-54.58876(2)	-54.58884(5)	-	-	-	$2s^22p^3$	$^4S^\circ$	-	-	-	-
	-54.50109(2)	-54.50118(3)	-54.50123(3)	0.08780(4)	0.08758(4)	0.08761(6)	$2s^22p^3$	$^2D^\circ$	0.087609	0.19(4)	-0.03(4)	0.00(6)
	-54.50108(3)	-54.501102(3)	-54.50120(5)	0.08781(4)	0.08766(2)	0.08764(7)	"	"	0.087609	0.21(4)	0.05(2)	0.03(7)
	-54.501034(1)	-54.501102(3)	-54.50119(2)	0.08786(2)	0.08766(2)	0.08766(5)	"	"	0.087609	0.25(2)	0.05(2)	0.05(5)
	-54.501034(1)	-54.50105(4)	-54.50119(2)	0.08786(2)	0.08772(5)	0.08766(5)	"	"	0.087609	0.25(2)	0.11(5)	0.05(5)
	-54.50092(3)	-54.50092(3)	-54.50115(3)	-	0.08785(4)	0.08769(6)	"	"	0.087609	-	0.24(4)	0.08(6)
	-54.45736313(2)	-54.45745(3)	-54.45745(3)	-	0.13140(2)	0.13140(6)	$2s^22p^3$	$^2P^\circ$	0.131401	-	0.00(2)	-0.00(6)
	-54.45736313(2)	-54.45742(1)	-54.45742(1)	-	0.13140(2)	0.13142(5)	"	"	0.131401	-	0.00(2)	0.02(5)
	-54.45721(3)	-54.45742(1)	-54.45742(1)	-	0.13156(4)	0.13142(5)	"	"	0.131401	-	0.16(4)	0.02(5)
	-54.20689(6)	-54.20798(3)	-54.20798(3)	-	0.38187(7)	0.38086(6)	$2s^22p^2(^3P)3s$	4P	0.379705	-	2.17(7)	1.16(6)
O	-75.0667572(6)	-75.06672(3)	-75.066849(9)	-	-	-	$2s^22p^4$	3P	-	-	-	-
	-75.0667572(6)	-75.066658(1)	-75.066849(9)	0.000000(9)	0.00006(3)	0.00000(1)	"	"	0.000000	0.0000(9)	0.06(3)	0.00(1)
	-75.066628(3)	-75.066658(1)	-75.06679(3)	0.00047(3)	0.00006(3)	0.00006(3)	"	"	0.000000	0.47(3)	0.06(3)	0.06(3)
	-74.99477(3)	-74.994713(3)	-74.99488(3)	0.07198(3)	0.07201(3)	0.07197(3)	$2s^22p^4$	1D	0.071944	0.04(3)	0.06(3)	0.02(3)
	-74.99466(3)	-74.994713(3)	-74.9947662(8)	0.07210(3)	0.07201(3)	0.072083(9)	"	"	0.071944	0.15(3)	0.06(3)	0.138(9)
	-74.99466(3)	-74.99466(5)	-74.99477(6)	-	0.07206(6)	0.07208(6)	"	"	0.071944	-	0.12(6)	0.14(6)
	-74.99461(5)	-74.9947662(8)	-74.9947662(8)	-	0.07211(6)	0.072083(9)	"	"	0.071944	-	0.17(6)	0.138(9)
	-74.99451(4)	-74.99471(6)	-74.99471(6)	-	0.07220(5)	0.07214(6)	"	"	0.071944	-	0.26(5)	0.20(6)
	-74.91306(3)	-74.91316(3)	-74.91316(3)	-	0.15366(5)	0.15369(3)	$2s^22p^4$	1S	0.153615	-	0.05(5)	0.07(3)
	-74.72779(8)	-74.72948(4)	-74.72948(4)	-	0.33893(9)	0.33737(4)	$2s^22p^3(^4S^\circ)3s$	$^5S^\circ$	0.335757	-	3.17(9)	1.61(4)
F	-99.73317(4)	-99.73293(7)	-99.73338(3)	-	-	-	$2s^22p^5$	$^2P^\circ$	-	-	-	-
	-99.73306(8)	-99.732819(2)	-99.73322(5)	0.00011(9)	0.00011(7)	0.00016(6)	"	"	0.000000	0.11(9)	0.11(7)	0.16(6)
	-99.73302(7)	-99.732819(2)	-99.73318(5)	0.00014(9)	0.00011(7)	0.00021(6)	"	"	0.000000	0.14(9)	0.11(7)	0.21(6)
	-99.26238(8)	-99.26406(7)	-99.26543(9)	0.47079(9)	0.4689(1)	0.4679(1)	$2s^22p^4(^3P)3s$	4P	0.466728	4.06(9)	2.1(1)	1.2(1)
	-99.26186(9)	-99.26347(8)	-99.26539(9)	0.4713(1)	0.4695(1)	0.4680(1)	"	"	0.466728	4.6(1)	2.7(1)	1.3(1)
	-99.26186(9)	-99.26334(8)	-99.26524(4)	-	0.4696(1)	0.46815(5)	"	"	0.466728	-	2.9(1)	1.42(5)
	-99.2537(1)	-99.255272(1)	-99.255272(1)	-	0.4792(1)	0.47811(3)	$2s^22p^4(^3P)3s$	2P	0.477070	-	2.1(1)	1.04(3)
	-99.25364(8)	-99.255272(1)	-99.255272(1)	-	0.4793(1)	0.47811(3)	"	"	0.477070	-	2.2(1)	1.04(3)
	-99.25335(8)	-99.25526(4)	-99.25526(4)	-	0.4796(1)	0.47813(5)	"	"	0.477070	-	2.5(1)	1.06(5)
	-99.1943(1)	-99.19580(6)	-99.19580(6)	-	0.5387(1)	0.53758(7)	$2s^22p^4(^3P)3p$	$^4P^\circ$	0.527905	-	10.8(1)	9.68(7)
Ne	-128.93712(5)	-128.93677(7)	-128.93707(4)	-	-	-	$2p^6$	1S	-	-	-	-
	-128.32430(6)	-128.3239(2)	-128.3243(3)	0.61282(8)	0.6129(2)	0.6128(3)	$2p^5(^2P_{3/2}^\circ)3s$	$^2[3/2]^\circ$	0.611453	1.37(8)	1.5(2)	1.4(3)
	-128.32405(6)	-128.3238(3)	-128.3243(3)	0.61307(8)	0.6130(3)	0.6128(3)	"	"	0.611453	1.61(8)	1.5(3)	1.4(3)
	-128.31737(6)	-128.3236(1)	-128.32422(6)	0.61975(8)	0.6131(1)	0.61285(7)	"	"	0.611453	8.30(8)	1.7(1)	1.40(7)
	-128.31712(7)	-128.31714(7)	-128.317581(1)	0.62000(9)	0.6196(1)	0.61949(

		FermiNet					Psiformer				
System	Term	Energy (Ha)	$\Delta\Delta E$ (mHa)	$\langle\hat{S}^2\rangle$	f	Δf	Energy (Ha)	$\Delta\Delta E$ (mHa)	$\langle\hat{S}^2\rangle$	f	Δf
BH	$^1\Sigma^+$	-25.28921(1)	-	0.000	-	-	-25.289249(9)	-	0.000	-	-
	-	-25.24045(2)	-	2.000	2.99e-07	-	-25.24047470(5)	-	2.000	1.13e-07	-
	-	-25.24043(1)	-	2.000	-2.21e-07	-	-25.24047470(5)	-	2.000	1.13e-07	-
	$^1\Pi$	-25.18376(3)	-0.38(3)	0.000	0.0236	-0.0004	-25.18386(1)	-0.44(1)	0.000	0.0235	-0.000513
	$^1\Pi$	-25.18374(2)	-0.36(3)	0.000	0.0239	-0.000129	-25.18383(1)	-0.42(1)	0.000	0.0239	-9.5e-05
HCl	$^1\Sigma^+$	-15.59729(1)	-	0.000	-	-	-15.597583(9)	-	0.000	-	-
	-	-15.32593(1)	-	2.000	-7.97e-08	-	-15.32633(1)	-	2.000	1.05e-06	-
	-	-15.32591(2)	-	2.000	-3.13e-08	-	-15.32632(1)	-	2.000	-9.45e-08	-
	$^1\Pi$	-15.30737(1)	-0.76(2)	0.000	0.0223	-0.000723	-15.3077421(5)	-0.846(9)	0.000	-9.78e-05	-0.0231
	$^1\Pi$	-15.30734(1)	-0.73(2)	0.000	0.0223	-0.000654	-15.3077421(5)	-0.846(9)	0.000	-9.78e-05	-0.0231
H ₂ O	1A_1	-76.43779(4)	-	0.000	-	-	-76.43809(2)	-	0.000	-	-
	3B_1	-76.16794(4)	0.48(6)	2.000	2.73e-06	-	-76.16844(2)	0.27(3)	2.000	5.9e-06	-
	1B_1	-76.15445(4)	0.00(6)	0.000	0.052	-3.28e-05	-76.15486(2)	-0.11(3)	0.000	0.0509	-0.00109
	3A_2	-76.09538(4)	0.65(6)	2.000	8.1e-06	-	-76.09583(3)	0.49(4)	2.000	-7.62e-07	-
	1A_2	-76.08935(4)	-0.31(6)	0.000	1.31e-05	-	-76.08974(3)	-0.40(4)	0.000	-7.14e-07	-
H ₂ S	1A_1	-11.38901(1)	-	0.000	-	-	-11.389308(8)	-	0.000	-	-
	3A_2	-11.17732(1)	0.74(1)	2.000	9.44e-07	-	-11.177684(9)	0.68(1)	2.000	3.09e-07	-
	3B_1	-11.17126(1)	-0.54(2)	2.000	7.27e-08	-	-11.171657(9)	-0.64(1)	2.000	8.94e-08	-
	1A_2	-11.16411(1)	0.73(1)	0.000	1.71e-06	-	-11.164486(9)	0.65(1)	0.000	1.4e-07	-
	1B_1	-11.15745(1)	-1.06(2)	0.000	0.059	-0.000967	-11.157900(9)	-1.21(1)	0.000	0.0596	-0.000401
BF	$^1\Sigma^+$	-124.67619(8)	-	0.000	-	-	-124.67772(3)	-	0.000	-	-
	-	-124.54200(1)	-	2.000	-2.9e-06	-	-124.5435944(6)	-	2.000	-1.12e-06	-
	-	-124.54200(1)	-	2.000	-2.9e-06	-	-124.5435944(6)	-	2.000	-1.12e-06	-
	$^1\Pi$	-124.44155(8)	-0.2(1)	0.001	0.231	-0.00295	-124.44351(3)	-0.62(4)	0.001	0.232	-0.00109
	$^1\Pi$	-124.4413(2)	0.0(2)	0.001	0.234	0.000532	-124.44339(3)	-0.50(4)	0.001	0.234	0.000644
CO	$^1\Sigma^+$	-113.32326(7)	-	0.001	-	-	-113.32477(3)	-	0.001	-	-
	-	-113.092094(2)	0.38(7)	2.000	5.61e-06	-	-113.094002(1)	-0.02(3)	2.000	-1e-06	-
	-	-113.092094(2)	0.38(7)	2.000	5.61e-06	-	-113.094002(1)	-0.02(3)	2.000	-1e-06	-
	$^1\Pi$	-113.01196(8)	0.4(1)	0.003	0.0837	0.00123	-113.0139(1)	-0.1(1)	0.001	0.0827	0.000196
	$^1\Pi$	-113.01183(8)	0.5(1)	0.002	0.0822	-0.000262	-113.0139(1)	0.0(1)	0.001	0.082	-0.000476
C ₂ H ₄	$^1B_{3u}$	-78.58542(6)	-	0.001	-	-	-78.58730(2)	-	0.001	-	-
	$^3B_{1u}$	-78.41786(6)	0.71(8)	2.000	1.65e-06	-	-78.41999(2)	0.46(4)	2.000	4.53e-06	-
	$^3B_{3u}$	-78.31636(6)	1.52(8)	1.997	7.95e-05	-	-78.31870(2)	1.07(4)	2.000	2.54e-05	-
	$^1B_{3u}$	-78.31239(6)	0.35(8)	0.005	0.0797	0.00368	-78.31493(2)	-0.32(4)	0.001	0.0792	0.00322
	$^1B_{1u}$	-78.29347(6)	1.63(8)	0.003	0.341	0.0028	-78.29640(3)	0.57(4)	0.002	0.343	0.00453
CH ₂ O	1A_1	-114.50546(8)	-	0.001	-	-	-114.50756(3)	-	0.001	-	-
	3A_2	-114.37336(7)	0.5(1)	2.001	1.57e-06	-	-114.37572(3)	0.27(5)	2.000	1.4e-06	-
	1A_2	-114.35941(7)	-0.6(1)	0.002	7.16e-07	-	-114.36179(3)	-0.86(5)	0.001	4.66e-07	-
	3B_2	-114.24138(8)	1.7(1)	1.996	4.37e-05	-	-114.24412(3)	1.05(5)	2.000	4.26e-06	-
	1B_2	-114.23587(8)	-0.1(1)	0.007	0.0272	0.00721	-114.23879(3)	-0.97(5)	0.002	0.0228	0.00275
CH ₂ S	1A_1	-49.45811(5)	-	0.002	-	-	-49.46048(2)	-	0.001	-	-
	3A_2	-49.38719(6)	-0.38(7)	2.000	1.1e-07	-	-49.38977(2)	-0.58(2)	2.000	7.14e-08	-
	1A_2	-49.37754(6)	-1.02(8)	0.002	3.9e-06	-	-49.37980(2)	-0.90(2)	0.001	1.47e-06	-
	3A_1	-49.33257(5)	-0.88(7)	2.000	6.61e-07	-	-49.33547(2)	-1.41(3)	2.000	6.96e-06	-
	3B_2	-49.23624(5)	10.19(7)	1.943	0.00387	-	-49.24069(2)	8.12(3)	1.999	0.000106	-
HNO	$^1A'$	-130.47995(7)	-	0.002	-	-	-130.48189(4)	-	0.001	-	-
	-	-130.44684(7)	-	2.000	7.95e-07	-	-130.44914(4)	-	2.000	3.24e-07	-
	$^1A''$	-130.41568(7)	0.7(1)	0.003	0.000379	-	-130.41808(5)	0.24(6)	0.002	0.000323	-
	$^1A'$	-130.25687(7)	64.3(1)	1.999	4.93e-05	-	-130.31268(7)	10.45(8)	0.010	6.55e-05	-
	-	-130.24429(8)	-	0.006	0.043	-	-130.25607(5)	-	1.729	0.00523	-
HCF	$^1A'$	-138.41429(9)	-	0.001	-	-	-138.41669(4)	-	0.001	-	-
	-	-138.37982(9)	-	2.000	-1.64e-09	-	-138.38220(4)	-	2.000	1.34e-06	-
	$^1A''$	-138.32289(9)	0.3(1)	0.002	0.00629	0.000286	-138.32567(4)	-0.12(6)	0.001	0.00631	0.000307
	-	-138.17085(9)	-	2.000	-4.98e-06	-	-138.17415(4)	-	1.999	6.26e-05	-
	-	-138.15756(9)	-	0.003	0.065	-	-138.16124(4)	-	0.002	0.0676	-
H ₂ CSi	1A_1	-43.11033(4)	-	0.001	-	-	-43.11183(1)	-	0.000	-	-
	-	-43.03848(4)	-	2.001	2.43e-06	-	-43.03986(1)	-	2.000	-4.87e-07	-
	1A_2	-43.03253(4)	-1.21(6)	0.001	1.04e-06	-	-43.03401(1)	-1.19(2)	0.001	1.35e-06	-
	-	-43.01749(4)	-	2.000	1.13e-05	-	-43.01966(1)	-	2.000	3.08e-06	-
	-	-43.00178(4)	-	2.000	5.48e-05	-	-43.00376(1)	-	2.000	6.31e-06	-

TABLE III: Energies, spin magnitudes, and oscillator strengths from the ground state for all systems in Fig. 2. The error in the vertical excitation energies ($\Delta\Delta E$) and oscillator strengths (Δf) relative to the theoretical best estimates^{45,46} are given as well.

Term	Energy (Ha)	$\langle \hat{S}^2 \rangle$	Oscillator strength f							
			$X^1\Sigma_g^+$	$a^3\Pi_u^-$	$a^3\Pi_u^+$	$c^3\Sigma_u^+$	$A^1\Pi_u^-$	$A^1\Pi_u^+$	$b^3\Sigma_g^-$	$B^1\Delta_g$
$X^1\Sigma_g^+$	-75.92258(2)	0.001	-	-0.00000	0.00000	0.00000	0.00373	0.00366	0.00000	0.00000
$a^3\Pi_u^-$	-75.91345(2)	2.000	-	-	0.00000	0.00000	0.00000	-0.00000	0.00300	0.00000
$a^3\Pi_u^+$	-75.91325(3)	2.000	-	-	-	0.00000	0.00000	0.00000	0.00308	0.00000
$c^3\Sigma_u^+$	-75.87881(3)	2.000	-	-	-	-	0.00000	0.00000	0.00000	-0.00000
$A^1\Pi_u^-$	-75.87752(2)	0.002	-	-	-	-	-	0.00000	0.00000	0.00250
$A^1\Pi_u^+$	-75.87733(3)	0.002	-	-	-	-	-	-	0.00000	0.00251
$b^3\Sigma_g^-$	-75.87527(3)	2.000	-	-	-	-	-	-	-	0.00000
$B^1\Delta_g$	-75.84563(3)	0.002	-	-	-	-	-	-	-	-

TABLE IV: Energies, spin magnitudes and oscillator strengths for the carbon dimer at equilibrium.

a/a_{eq}	$X^1\Sigma_g^+$	$a^3\Pi_u$	$b^3\Sigma_g^-$	$c^3\Sigma_u^+$	$A^1\Pi_u$
0.8	-75.77419(4)	-75.69933(2)	-	-75.75841(4)	-75.66008(2)
0.9	-75.89507(3)	-75.8582840(1)	-	-75.86532(3)	-75.82059(1)
0.95	-75.91682(3)	-75.89481(1)	-	-75.87997(3)	-75.8580627(1)
1.0	-75.92258(2)	-75.91335(1)	-75.87527(3)	-75.87881(3)	-75.87743(1)
1.05	-75.91770(2)	-75.91940(1)	-75.88916(3)	-75.86724(3)	-75.8842239(4)
1.1	-75.90569(3)	-75.9170(5)	-75.89303(3)	-75.84916(3)	-75.8817(1)
1.2	-75.87094(3)	-75.8941956(8)	-75.88248(3)	-	-75.861694(1)
1.3	-	-75.86264(1)	-75.85935(3)	-	-
1.4	-	-75.8296(3)	-75.83243(2)	-	-
1.5	-	-75.79841(1)	-75.80516(3)	-	-

TABLE V: Potential energy curves for different states of the carbon dimer. Energies whose state could not be unambiguously identified from their symmetries are omitted. Π states are doubly-degenerate and the average energy is given here. Bond lengths are reported as multiples of the equilibrium length of 1.244Å. Energies are in atomic units.

	FermiNet		Psiformer	
	Energy (Ha)	$\langle \hat{S}^2 \rangle$	Energy (Ha)	$\langle \hat{S}^2 \rangle$
$\tau=0, k=5$	-78.58389(7)	0.002	-78.58629(3)	0.001
	-78.42187(7)	2.000	-78.42446(3)	2.000
	-78.31728(6)	1.996	-78.32053(3)	2.000
	-78.31335(6)	0.007	-78.31663(3)	0.001
	-78.29620(7)	0.005	-78.29949(3)	0.002
$\tau=0, k=3$	-78.58465(6)	0.001	-78.58626(3)	0.001
	-78.42296(6)	2.000	-78.42424(3)	2.000
	-78.31716(6)	1.413	-78.31874(3)	0.001
$\tau=15$	-78.58083(6)	0.001	-78.58161(3)	0.001
	-78.42683(6)	2.000	-78.42763(3)	2.000
	-78.31128(6)	0.002	-78.31227(4)	0.004
$\tau=30$	-78.56795(6)	0.001	-78.56930(3)	0.001
	-78.43636(6)	2.000	-78.43774(3)	2.000
	-78.33266(6)	0.002	-78.33452(3)	0.002
$\tau=45$	-78.54724(5)	0.001	-78.54852(3)	0.001
	-78.44801(6)	2.000	-78.44929(3)	2.000
	-78.35192(6)	0.002	-78.35327(3)	0.002
$\tau=60$	-78.51944(6)	0.001	-78.52094(3)	0.001
	-78.45856(5)	2.000	-78.45999(3)	2.000
	-78.36711(6)	0.002	-78.36861(3)	0.002
$\tau=70$	-78.49858(6)	0.001	-78.50006(3)	0.001
	-78.46394(6)	2.000	-78.46536(3)	2.000
	-78.37368(6)	0.002	-78.37585(3)	0.001
$\tau=80$	-78.47919(5)	0.001	-78.48064(3)	0.001
	-78.46745(5)	2.000	-78.46873(3)	2.000
	-78.37756(5)	0.002	-78.37959(3)	0.002
$\tau=85$	-78.47247(6)	0.001	-78.47399(3)	0.001
	-78.46819(6)	2.000	-78.46973(3)	2.000
	-78.38004(6)	0.001	-78.38159(3)	0.001
$\tau=90$	-78.46991(6)	0.003	-78.47133(3)	0.003
	-78.46851(6)	1.999	-78.47001(3)	1.998
	-78.38188(6)	0.001	-78.38337(3)	0.001
$\phi=0.0$	-78.47283(5)	0.009	-78.47409(2)	0.003
	-78.47116(5)	1.993	-78.47243(2)	1.998
	-78.38395(5)	0.001	-78.38519(3)	0.001
$\phi=20.0$	-78.47176(5)	0.001	-78.47289(2)	0.001
	-78.47033(5)	2.000	-78.47151(2)	2.000
	-78.38669(5)	0.001	-78.38824(3)	0.001
$\phi=40.0$	-78.46626(5)	0.042	-78.46735(3)	0.006
	-78.46555(5)	1.960	-78.46678(3)	1.995
	-78.39383(5)	0.001	-78.39510(3)	0.001
$\phi=60.0$	-78.45258(5)	1.923	-78.45374(3)	2.034
	-78.45231(5)	0.078	-78.45340(3)	-0.033
	-78.40003(5)	0.001	-78.40135(3)	0.001
$\phi=70.0$	-78.44149(5)	1.993	-78.44278(3)	1.987
	-78.44051(5)	0.009	-78.44196(3)	0.014
	-78.40085(5)	0.001	-78.40234(3)	0.001
$\phi=80.0$	-78.42701(5)	2.000	-78.42815(3)	1.999
	-78.42552(5)	0.002	-78.42664(3)	0.002
	-78.39926(5)	0.001	-78.40073(3)	0.001
$\phi=90.0$	-78.40856(6)	2.002	-78.40991(3)	2.000
	-78.40621(6)	-0.000	-78.40779(3)	0.001
	-78.39454(6)	0.001	-78.39591(1)	0.001
$\phi=95.0$	-78.39794(5)	2.000	-78.39952(3)	1.999
	-78.39555(5)	0.001	-78.39676(3)	0.002
	-78.39079(5)	0.001	-78.39205(3)	0.001
$\phi=97.5$	-78.39275(5)	2.000	-78.39400(3)	2.000
	-78.38973(5)	0.001	-78.39106(3)	0.001
	-78.38829(5)	0.002	-78.38996(3)	0.001
$\phi=100.0$	-78.38690(5)	2.002	-78.38826(3)	2.005
	-78.38587(5)	-0.000	-78.38728(3)	-0.003
	-78.38350(5)	0.002	-78.38503(3)	0.001
$\phi=102.5$	-78.38331(5)	-0.001	-78.38445(3)	0.003
	-78.38113(5)	2.002	-78.38248(3)	1.998
	-78.37771(5)	0.002	-78.37894(3)	0.001
$\phi=105.0$	-78.38000(5)	0.001	-78.38142(3)	0.001
	-78.37507(6)	2.000	-78.37652(3)	2.000
	-78.37125(6)	0.002	-78.37267(3)	0.001
$\phi=110.0$	-78.37315(5)	0.001	-78.37458(3)	0.001
	-78.36317(5)	1.999	-78.36440(3)	2.000
	-78.35850(5)	0.003	-78.35975(3)	0.001
$\phi=120.0$	-78.35644(6)	0.001	-78.35776(3)	0.001
	-78.33870(6)	2.000	-78.34010(3)	1.999
	-78.33257(6)	0.001	-78.33368(3)	0.002

TABLE VI: Energies and spin magnitudes for the lowest states of twisted ethylene using the FermiNet and Psiformer Ansätze. Note that for the FermiNet at $\tau = 0$, the singlet and triplet states are mixed together when $k=3$, so we compute $k=5$ at that geometry only.

State	FermiNet			Psiformer			Entwistle <i>et al.</i> ¹⁸			DMC ¹⁷	CASPT2 ⁶⁶	TD-DFT ⁶⁵	TBE ⁵⁰
	Energy (Ha)	ΔE	$\langle \hat{S}^2 \rangle$	Energy (Ha)	ΔE	$\langle \hat{S}^2 \rangle$	Raw	σ^2	Match	ΔE	ΔE	ΔE	ΔE
¹ <i>A</i> _{1g}	-232.1898(2)	-	0.017	-232.23323(8)	-	0.008	-232.0675(11)	-232.0265(13)	-	-	-	-	
³ <i>B</i> _{1u}	-232.0324(2)	157.4(3)	2.007	-232.07790(9)	155.3(1)	2.003	-231.8628(9)	-231.8628(9)	152(1)	145	140	153	
³ <i>E</i> _{1u}	-232.0071(2)	182.7(3)	1.994	-232.0535(1)	179.3(1)	2.002	-	-	180(1)	165	173	179	
³ <i>E</i> _{1u}	-232.0056(2)	184.2(3)	1.968	-232.0531(1)	180.1(1)	1.996	-	-	182(1)	165	173	179	
¹ <i>B</i> _{2u}	-231.9995(2)	190.3(3)	0.078	-232.04581(9)	187.4(1)	0.021	-	-	189(1)	173	198	186	
³ <i>B</i> _{2u}	-231.9586(2)	231.2(3)	1.126	-232.01686(9)	216.4(1)	1.993	-	-	216(1)	200	185	213.5	

TABLE VII: Energies and spin magnitudes for the excited states of benzene using the FermiNet and Psiformer Ansätze, with comparison against QMC penalty methods^{17,18}, CASPT2⁶⁶ and TD-DFT⁶⁵ and theoretical best estimates from coupled cluster⁵⁰. All relative energies from the ground state (ΔE) are given in milli-Hartrees. For the highest excited state of the FermiNet, inspection of the spin magnitude reveals contamination by the singlet ¹*B*_{1u} state, which would explain the anomalously high energy. The Psiformer does not suffer from this contamination.